Science of the Total Environment 648 (2019) 1105–1120

Contents lists available at ScienceDirect

Science of the Total Environment

journal homepage: www.elsevier.com/locate/scitotenv

Hydrogeophysical characterization and monitoring of the hyporheic and riparian zones: The Vermigliana Creek case study

Laura Busato [a,*], Jacopo Boaga [a], Maria Teresa Perri [a], Bruno Majone [b], Alberto Bellin [b], Giorgio Cassiani [a]

[a] Department of Geosciences, University of Padova, Via Giovanni Gradenigo 6, 35131 Padova (PD), Italy
[b] Department of Civil, Environmental and Mechanical Engineering, University of Trento, Via Mesiano 77, 38123 Trento (TN), Italy

HIGHLIGHTS

- Hyporheic and riparian zones are usually studied by means of punctual methods.
- Geophysical acquisitions lead to 2D data distributions under the creek.
- The geophysical cables are placed under the creek, in the domain of interest.
- Geophysical and hydrological data are merged to calibrate a flow-transport model.
- Different subdomains are highlighted: sub-riverbed, left and right banks.

GRAPHICAL ABSTRACT

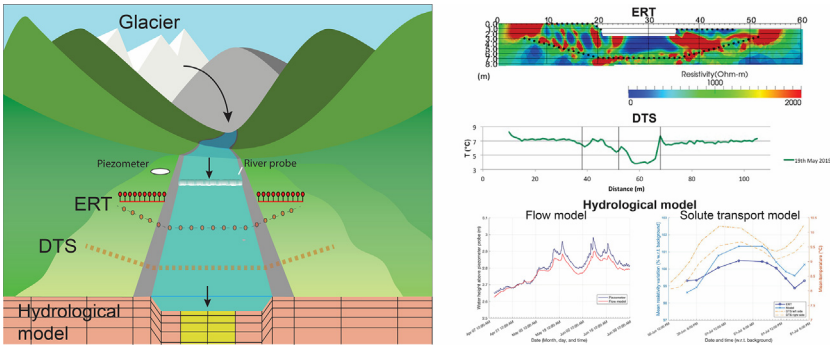

ARTICLE INFO

Article history:
Received 8 June 2018
Received in revised form 13 August 2018
Accepted 14 August 2018
Available online 16 August 2018

Editor: D. Barcelo

Keywords:
Instrumentation under the riverbed
Semi-horizontal boreholes
Electrical resistivity tomography
Distributed temperature sensing
Flow and transport modeling

ABSTRACT

The hyporheic and riparian zones are critical domains in a river ecosystem since they mediate the interactions between surface water and groundwater. These domains are generally strongly heterogeneous and difficult to access; yet their characterization and monitoring still rely mostly on hard-to-perform invasive surveys that provide only point information. These well-known issues, however, can be overcome thanks to the application of minimally invasive methods. In this paper, we present the results of the hydrogeophysical characterization of the Vermigliana Creek's hyporheic and riparian zones, performed at an experimental site in the Adige catchment, northern Italy, by means of electrical resistivity tomography (ERT), distributed temperature sensing (DTS), and hydrological modeling. A major advancement is given by the placement of electrodes and of an optical fiber in horizontal boreholes at some depth below the river bed, put in place via directional drilling. The results of this static and dynamic (time-lapse) geophysical characterization identify the presence of two subdomains (the sub-riverbed and the left and right banks) and define the water flow and solute dynamics. The ERT information is then used, together with other hydrological data, to build a 3D subsurface hydrological model (driven mainly by the watercourse stage variations) that is calibrated against local piezometric information. A solute transport model is then developed to reproduce the variations observed in the dynamic geophysical monitoring. The results show good agreement between ERT data and the model outcome. In addition, the transport model is also consistent with the temperature data derived from DTS, even though some slight discrepancies show that the heat capacity of the solid matrix and heat conduction cannot be totally neglected.

Abbreviations: ERT, electrical resistivity tomography; DTS, distributed temperature sensing.

* Corresponding author at: Interdepartmental Center for Environmental Research – C.I.R.AM., University of Naples Federico II, Via Mezzocannone 16, 80134 Naples (NA), Italy.
E-mail address: laura.busato.3@gmail.com (L. Busato).

https://doi.org/10.1016/j.scitotenv.2018.08.179
0048-9697/

1. Introduction

The hyporheic zone is the transition region where the interactions between surface water and groundwater take place (Orghidan, 2010; Reidy and Clinton, 2004). This domain, together with the riparian zones, allows the transport of several substances (including water, nutrients and pollutants) from a stream to the underlying aquifer, and vice versa, thus playing a fundamental role in the river ecosystem (Boulton et al., 1998). Having a strong interconnection with human activity, the interchange phenomena that occur in the hyporheic and riparian zones represent a target of study shared by several disciplines, which range from hydraulics (Greswell, 2005), to biogeochemistry and ecology (Bridge, 2005). These fields of study rely on methods that are usually invasive and based on sample analysis (for further details see Bridge, 2005; Greswell, 2005), and are likely not to sample the domain with the necessary spatial resolution given the strong heterogeneity of these systems and the difficulty to access them. A major step forward can be provided by the application of minimally-invasive geophysical techniques: these cost-effective and relatively fast methodologies, in fact, if adequately combined with flow and transport models, allow the evaluation and monitoring of surface/subsurface structures and processes at different scales, both in terms of time and space, as shown by the fast development of *hydrogeophysics* (e.g. Binley et al., 2010, 2015; Rubin and Hubbard, 2005).

One of the most commonly employed techniques is electrical resistivity tomography (ERT; e.g. Daily et al., 2004), both from the surface (e.g., Nyquist et al., 2008) and in boreholes (e. g., Crook et al., 2010). Based on Ohm's law and on the principle that the distribution of the electrical voltage on the earth surface or underground (around a current-carrying electrode) depends on the medium electrical resistivity (ρ) (as well as on the source characteristics), ERT allows to obtain 2D/3D images of the subsurface electrical resistivity distribution. Since the spatial (and temporal) variations in electrical resistivity are affected by lithology, pore fluid chemistry, and water content, the ERT method has a significant potential for hydrogeophysical applications, particularly to study time-dependent processes (Binley and Kemna, 2005). This is the reason why ERT, and in particular its application in the time-lapse mode, has been one key methodology for hydrogeophysical imaging over the last two decades. Another promising methodology in static and dynamic subsurface characterization is represented by distributed temperature sensing (DTS; e.g. Selker et al., 2006; Tyler et al., 2009). This is a technique of investigation (active or passive) that allows measuring temperature (T) by means of a fiber optic cable, which acts as a linear temperature sensor and is based on the Raman scattering effect (Graves and Gardiner, 1989; Raman and Krishnan, 1928). This effect represents one of the various scattering phenomena that originate from the interaction between photons and molecules of the fiber optic and leads to a backscattered signal whose intensity is temperature-dependent (see Selker et al., 2006). Such signal can therefore be properly detected and processed in order to determine the variation of temperature along the cable itself. The position of the temperature reading is determined by measuring the arrival time of the returning light pulse, so the result is a continuous temperature profile along the entire length of the sensor cable, with spatial resolution (along the cable) in the meter range. This method allows to exploit heat as a tracer (Anderson, 2005; Constantz, 2008) and, therefore, to observe temperature variations both in terms of space and time.

These geophysical methods (ERT and DTS) are state-of-the-art in the hydrogeophysical field and have already been used to characterize the hyporheic and riparian zones. As a matter of fact, several studies have shown the capabilities of ERT to image the riparian zone (e.g. Busato et al., 2016; Perri et al., 2018; Vignoli et al., 2016). Coscia et al. (2012) present a 3D time-lapse ERT monitoring by means of vertical boreholes in the riparian zone, while Nyquist et al. (2008, 2009) focus on stream bottom and lakebed ERT characterization, in the latter case also in combination with temperature measurements. Other examples comprise 3D ERT acquisitions from the surface to monitor surface water-groundwater interactions (Johnson et al., 2012), or in boreholes using the river water as tracer (Coscia et al., 2011), while Cardenas and Markowski (2010) present a 2D ERT time-lapse monitoring with electrodes placed on the streambed and partly also on the adjacent soil surface. With regard to the DTS, despite being a relatively recent technique in the hydrogeophysical field (e.g. Hurtig et al., 1996), many applications are available in the literature: some authors investigated the surface water-groundwater interactions placing the fiber-optic cable on the riverbed, also in contaminated contexts (e.g. Anderson et al., 2014; Briggs et al., 2012a, 2013; Mwakanyamale et al., 2012; Slater et al., 2010; Voytek et al., 2014; Westhoff et al., 2011), while others opted for vertical boreholes, with the fiber-optic cables wrapped around a PVC tube (e.g. Briggs et al., 2012b; Vogt et al., 2010). Although all these pieces of work demonstrate the wide applicability of both ERT and DTS for a better characterization of the regions surrounding a riverbed, literature lacks (to the best of our knowledge) of studies where the instrumentation is located beneath the riverbed, i.e. directly inside and/or surrounding the hyporheic zone where the exchanges between surface water and groundwater occur.

In this work, we present an innovative instrumentation set-up where part of the instrumented cables is placed below the riverbed and put in place via directional, semi-horizontal, drilling. This instrumentation arrangement has not been reported to have been deployed yet for similar purposes and can lead to major improvements in the spatial characterization of the hyporheic and riparian zones. The best way to fully exploit hydrogeophysical data is through the development of a hydrological model. Several examples of hyporheic and riparian zones models can be found in the literature (e.g. Fleckenstein et al., 2010; Gooseff et al., 2006; Lautz and Siegel, 2006; Siergieiev et al., 2015; Tonina and Buffington, 2007), with some of them involving a comparison against ERT acquisitions (e.g. Doetsch et al., 2012; Doro et al., 2013; Ward et al., 2010, 2013) or temperature measurements (Bianchin et al., 2010; Dugdale et al., 2017; Westhoff et al., 2007). In this work, however, we use the ERT data (in combination with other hydrological information) not only to identify different materials in the mesh, but also to determine the best set of hydrological parameters that describe these materials by comparing the ERT hydrogeophysical information with the outcomes of a solute transport model. The study was conducted as part of the EU FP7 projects CLIMB (Ludwig et al., 2010) and GLOBAQUA (Navarro-Ortega et al., 2015). The attention is focused on the Vermigliana Creek catchment, which is part of the Adige River catchment (Trentino-Alto Adige Region, Italy).

In view of the above, the aim of this paper is to present a study where we use a combination of geophysical and hydrological techniques to understand the interconnection between surface water and groundwater, which represents a fundamental step in the development of an effective water-resource management plan. Therefore, the main objectives of this research are:

a) to delineate the subsurface hydrogeologic structures that form the hyporheic and riparian zones of the Vermigliana Creek;
b) to monitor the hydrogeological processes that take place in the hyporheic and riparian zones with unprecedented high spatial resolution capabilities, in order to collect data useful to understand the role of the hyporheic zone in the river ecosystem; and
c) to combine ERT and hydrological data in the development of a flow and solute transport model aimed at describing the sub-riverbed domain.
d) to assess to what extent the information content of DTS and ERT, both acquired using the novel geometry in the hyporheic zone, can be compared.

2. The Vermigliana creek field site

The site chosen for this study is located along the Vermigliana Creek, near the small village of Vermiglio (Val di Sole valley, Trento, Italy). In

particular, the site is placed in correspondence to a hydrological station, at approximately 1200 m above mean sea level, close to a bridge crossing the stream and in proximity of two small lakes (Fig. 1), whose emissary connects them with the creek just downstream of the station. In this portion of the creek, the riverbed is characterized by the presence of a pit, just below the bridge, which creates a small waterfall (Fig. 2b).

The Val di Sole presents a mountain climate, characterized by short and cool summers and long winters (with abundant snowfall precipitations). However, given the complex orography of the area, such climatic aspects do not depend only on the general dynamics, but also on local factors, among which altitude and soil cover. Precipitation values have a minimum in winter and two maxima in spring and autumn, whereas total annual values increase with altitude. The hottest months are July and August in the whole area, while the coldest month is January in the valley bottom and February at high altitudes. Furthermore, the average thermal values decrease with altitude. Lastly, the presence of snow cover characterizes the period comprised between the months of November and May (the duration of which increases with altitude; Blokhina, 2014).

The Vermigliana Creek is a tributary of the Noce River, and it originates from the Alpine glaciers of Presanella and Cevedale (at 1.882 m AMSL) and ends at Cusiano (at 942 m AMSL). Its watercourse, which flows through a basin of 78.95 km^2, has several tributaries, some originating from the Presena Glacier as well, while others are minor creeks fed by rain drainage and snow melting processes. The hydrological regime of the Vermigliana Creek is typically Alpine, with strong and abrupt flow variations. The lean season occurs during winter, while the flow rates increase is caused by the snow/ice melting occurring in spring and early summer.

Inside the Vermigliana basin, the altitude values are comprised between 1175 and 3540 m above mean sea level and the landscape is typical of an alpine glacial valley, with the characteristic U-shaped cross-section and steep slopes. The average slope of the creek at Vermiglio section is 47.3 m/km, but the riverbed slope decreases toward the last stretch of the creek, often causing flooding (Blokhina, 2014). From a geological point of view, the Vermigliana Creek basin is located at the border of two large structural units of the Alps: the Austroalpine unit and the Southern Limestone Alps. This boundary consists of a tectonic faults system called Insubric Line (or Tonale Line in this geological region), which crosses the Val di Sole longitudinally (Castellarin et al., 2005). The Vermigliana basin is, therefore, mainly composed of metamorphic rocks that, from a hydrogeological point of view, have limited secondary permeability due to fracturing processes or along the discontinuity lines (Dal Piaz et al., 2007). More in detail, the valley through which the Vermigliana Creek and its tributaries flow has a sillimanite bearing gneiss bedrock that underlays glacial and alluvial deposits, whose thickness varies from a few to about 10 m (Fig. 3c; Dal Piaz et al., 2007). These deposits, identified as the "postglacial alpine synthem" (Dal Piaz et al., 2007), can be classified as glacial till and consist in poorly sorted diamicton containing gravel and boulders, suspended in a matrix of sand and clay. This material forms unconfined aquifers that are connected to the sub-stream water circulation (Dal Piaz et al., 2007). The system's response hence depends on internal factors, such as geometry and hydraulic conductivity of the fractured-porous domain. In particular, the superficial component of the outflow is the result of the following conditions: (i) the basin is developed on low-permeable formations; and (ii) the riverbed is built upon a high fractured medium. Total saturation is quickly reached, regardless of the geometry and hydraulic conductivity of the fluvio-glacial deposits (Blokhina, 2014).

3. Methods: applied geophysics and hydrological modeling

As introduced in Section 1, in this specific case study ERT and DTS are used as field methodologies, as they allow a high-resolution characterization of the hyporheic and riparian zones, overcoming the critical problem of measuring quantities under the riverbed. In particular, our non-conventional acquisition geometry (Fig. 2b) for both ERT and DTS enhances dramatically the imaging capabilities of ERT and the sampling capabilities of DTS at depth. In addition to this, traditional hydrological

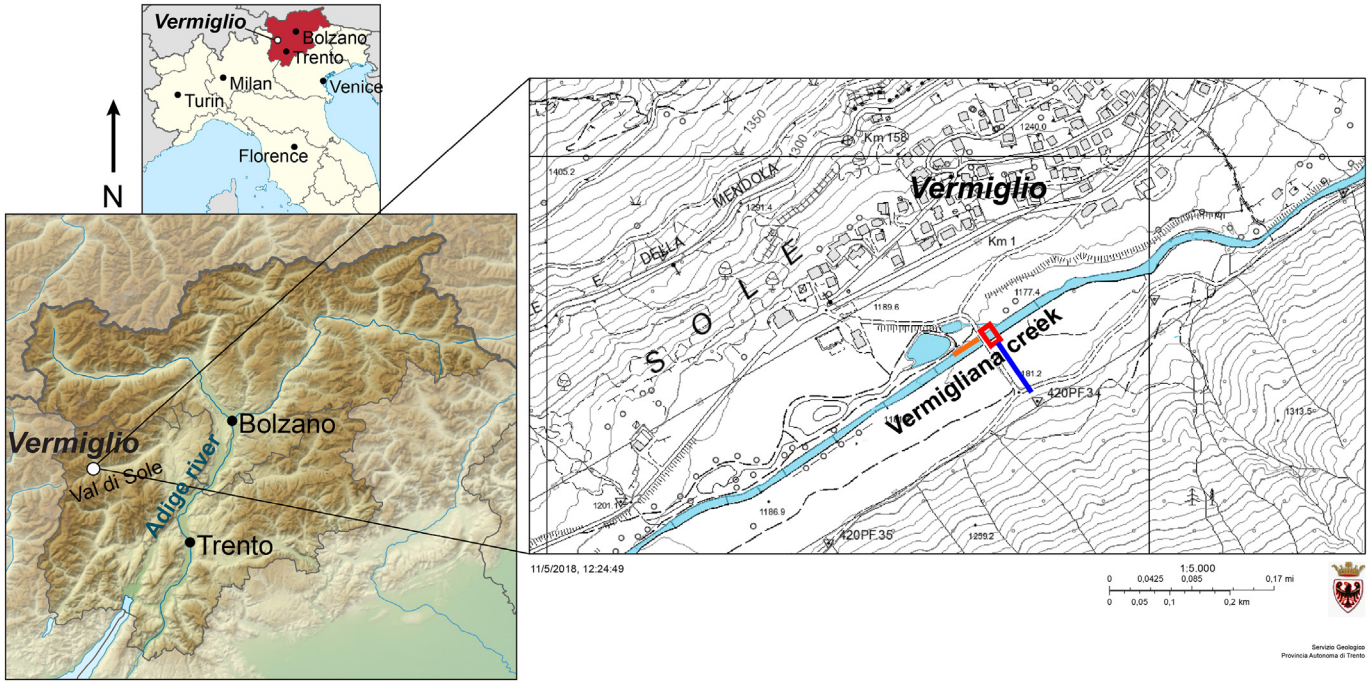

Fig. 1. Study site near the small village of Vermiglio (Val di Sole, province of Trento, Adige River catchment). The Vermigliana creek and the two small lakes are highlighted in light blue. The red rectangle locates the area investigated by the ERT and DTS acquisitions, whereas the blue solid line and the orange solid line indicate the auxiliary GPR and ERT acquisitions, respectively. The technical map of the province on the right (Carta Tecnica Proviciale, CTP) is provided by the Servizio Geologico – Provincia autonoma di Trento (2017). (For interpretation of the references to colour in this figure legend, the reader is referred to the web version of this article.)

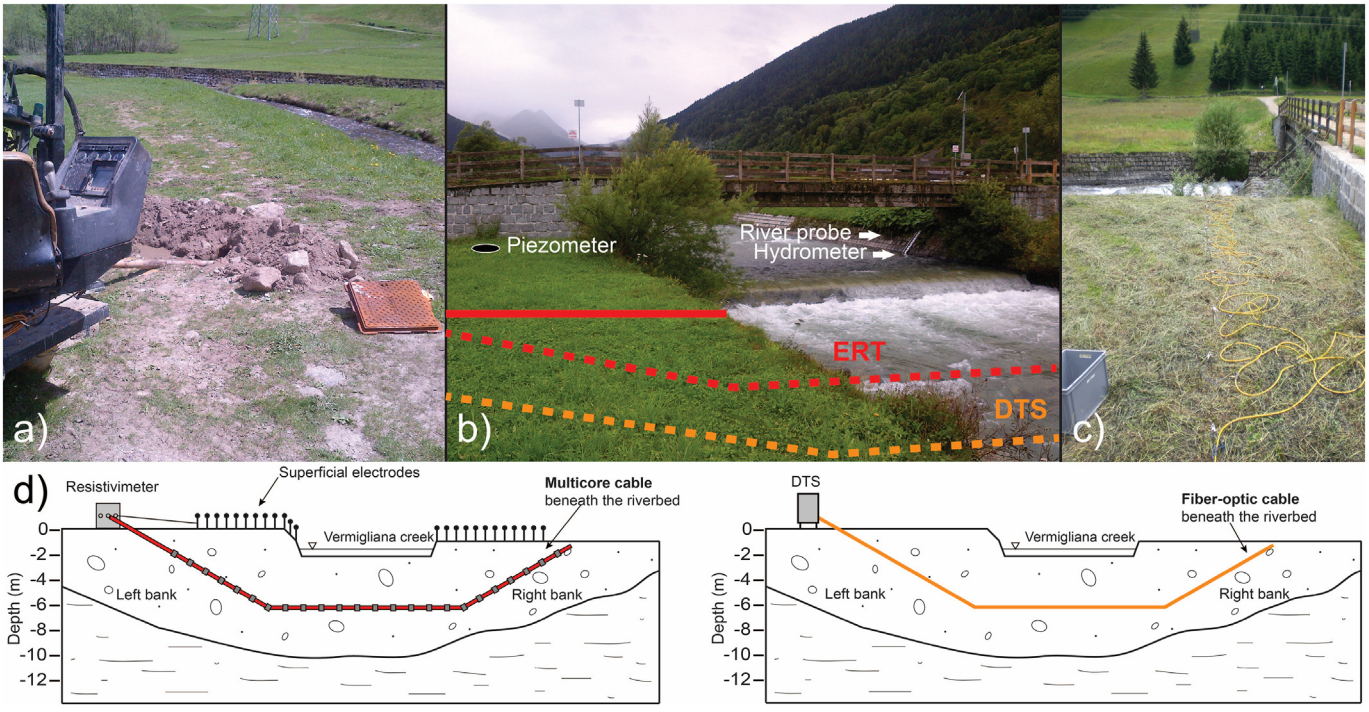

Fig. 2. a) Oriented borehole drilling at the Vermigliana site; b) scheme of instrumentation deployment: ERT superficial cable location on the right bank (red solid line. Please, note that the same instrumentation disposition is present also on the left bank); ERT borehole cable placed 5 m under riverbed (red dashed line); and DTS fiber-optic cable, parallel to the ERT borehole line; c) detail of the superficial electrodes on the left embankment; and d) schemes representing the position of the ERT and DTS instruments in the sub-riverbed at the Vermiglio section. The schemes are not to scale. (For interpretation of the references to colour in this figure legend, the reader is referred to the web version of this article.)

monitoring at the river gauging station is warranted by two multi-parameter probes (Aqua TROLL 200 Data Logger, In-Situ Inc.) that measure water level, electrical conductivity, and temperature of the river water and in a piezometer located on the left bank of the creek (Fig. 2b). The ERT and hydrological data thus obtained are then used to develop a hydrological model.

3.1. Geophysical instrumentation placement beneath the riverbed

The ERT and DTS cables positioning under the riverbed was performed thanks to the directional boring technique, a trenchless method that allows the drilling of sub-horizontal boreholes. At our field site we opted for a Ditch Witch JT3020 directional drill, which was placed on

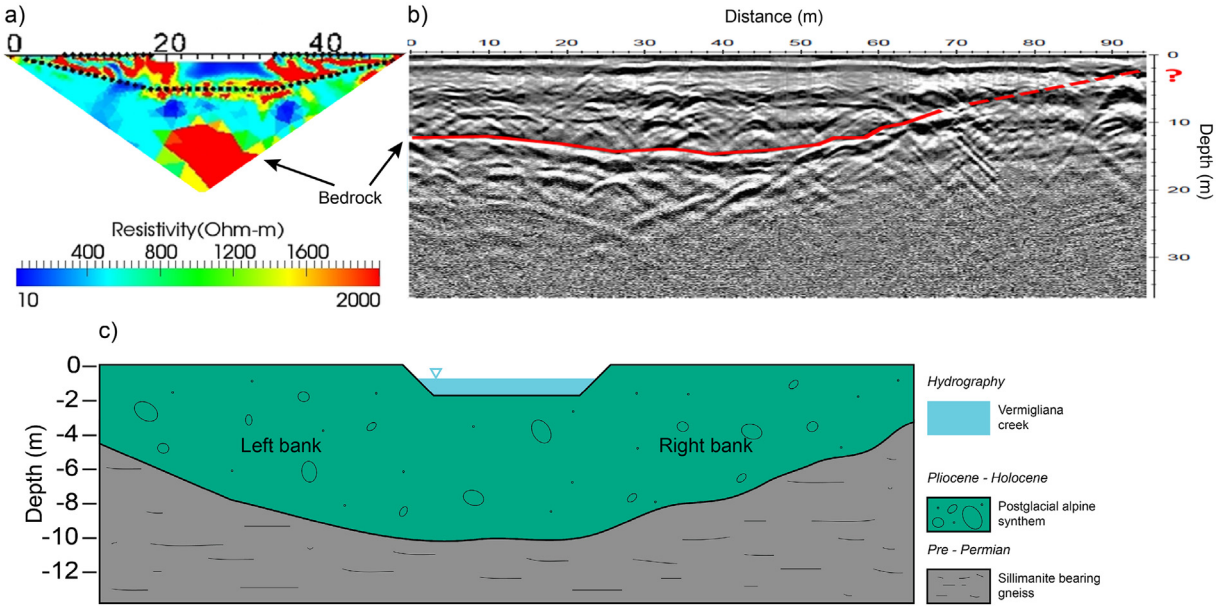

Fig. 3. Comparison between a) the resistivity cross-section resulting from the static inversion of July 2, 2013 ERT acquisition, b) the radargram obtained from the October 6, 2011 measurement, and c) a schematic geological cross-section of the Alta Val di Sole in correspondence of the Vermiglio field site (Dal Piaz et al., 2007). The red solid line in the radargram locates a strong reflector, which may be interpreted as the bedrock, whose depth agrees with both the high resistivity domain in the ERT image and the geological features of the area described by Dal Piaz et al., 2007. The schematic geological cross-section is not to scale with respect to the ERT section and the radargram. (For interpretation of the references to colour in this figure legend, the reader is referred to the web version of this article.)

the left bank of the Vermigliana creek (Fig. 2a) to drill two different boreholes, one for the ERT cable and one for the DTS fiber-optic. In both cases, the position of the drilling head was monitored throughout the whole process by means of a locating system, in order to have a more precise perforation. Once the borehole was drilled, the drilling head was replaced with a backreamer, which, in turn, was connected to several PVC pipes (DN90 with internal diameter equal to 73.6 mm). As the reamer was pulled backwards following the same path dug by the drilling head, the PVC pipes were installed within the borehole as support. Then, the ERT and DTS cables were inserted inside the pipes in the corresponding borehole and, finally, the PVC tubes were removed to let the soil collapse on the cables themselves. This guarantees a good contact since both the electrodes and the fiber-optic are enclosed within the soil (Fig. 2d). Moreover, the placement of the cables beneath the river bed took place a few weeks prior to the beginning of the geophysical monitoring to ensure a better coupling between the instrumentation and the soil. Note also that, in the particular case at hand, both electrode cable and DTS optical fiber are placed in the saturated portion of the unconfined aquifer, thus both electrical contact and heat transfer are greatly facilitated.

3.2. Electrical resistivity tomography (ERT)

The ERT data allow for two different types of inversions: absolute inversion and time-lapse inversion. When the attention is focused on absolute (or static) information, only a single absolute image of electrical resistivity distribution is obtained: this approach is useful for deriving static information of subsoil (e.g., delineation of lithological boundaries and layers geometry). Conversely, in order to gather dynamic information about sub-surface processes, time-lapse monitoring and inversion are needed. Resistivity imaging surveys are hence repeated over the same position at different times, thus allowing the user to distinguish between static and dynamic effects (for further details regarding this method please refer to, e.g. Binley, 2015; Binley and Kemna, 2005).

3.2.1. Acquisition scheme and data processing

In the Vermigliana ERT set-up we used 72 electrodes: the survey scheme is composed of a multicore cable with 48 brass electrodes spaced 1 m, placed (in the central part) 5 m beneath the riverbed, i.e. inside the domains of interest in this study, and 24 stainless steel surface electrodes spaced 1 m (12 on each river side, Fig. 2b, c, and d). The chosen acquisition scheme is a skip zero dipole–dipole configuration (i.e. a configuration where the electrodes of both current and potential dipoles have the minimum possible distance): this set-up ensures maximal spatial resolution provided that the signal-to-noise ratio is sufficiently high. The data quality is assessed using a full acquisition of both direct and reciprocals measurements to estimate the data error, on the basis of the principle of reciprocity (see e.g. Binley et al., 1995; Monego et al., 2010), which states that the current and potential electrodes can theoretically be interchanged without affecting the measured resistance (the ratio between voltage and current). A total of roughly 4800 measurements was then collected during each ERT acquisition using a Syscal Pro 72 resistivity meter (Iris Instruments). However, when dealing with real datasets, the resistance value measured by each direct quadrupole differs from the value measured by the corresponding reciprocal one. This allows to associate each direct-reciprocal couple to the corresponding relative error, in order to remove those pairs whose error exceeds a certain threshold, in this work equal to 10%. Determining the error level is crucial when dealing with an Occam type inversion such as that implemented in the R2 code (Binley, 2016) used in this work, as discussed e.g. by LaBrecque et al. (1996). With regard to the time-lapse inversion, the analysis of the resistivity variations with time was performed following the method of Daily et al. (1992) (for further details see also Cassiani et al., 2006).

3.2.2. Measurement campaigns

The ERT measurements aimed at characterizing the hyporheic zone of the Vermigliana creek can be divided into two types of datasets: the seasonal monitoring, with one acquisition every two or three weeks, and the short-term monitoring, with a measurement approximately every 2 h. With respect to the seasonal monitoring, several ERT acquisitions have been performed in 2013 and 2015 taking advantage of the snow-free season (from Spring to early Autumn). On the contrary, the short-term monitoring took place only between June 30 and July 1, 2015. Dates and times of both seasonal and short-term monitoring are summarised in Tables 1 and 2, respectively.

3.3. Distributed temperature sensing (DTS)

3.3.1. Acquisition scheme

The DTS measurements have been conducted using an AP Sensing (N43866A) instrument, with a double–ended fiber–optic configuration (i.e. both ends of the cable are connected to the instrument), with a spatial resolution equal to roughly 1 m and precision equal to 0.1 °C. In each survey, we acquired three single traces with update time and measurement time both equal to 30 s (i.e., every 30 s a new trace acquisition begins and lasts for 30 s) and we averaged the three temperature values thus obtained for every sampling point: the result consists of a single profile with temperature data spaced 1 m from each other.

3.3.2. Measurement campaigns

Several DTS surveys took place in 2013 and 2015 in correspondence of the ERT measurements, so as to obtain complete seasonal and short-term datasets also for this methodology (see Tables 1 and 2 for detailed dates and times. Please note that the lack of measurements on July 24, 2015 and August 27, 2015 is due to an instrument failure).

3.4. Auxiliary geophysical investigations

The geophysical characterization of the Vermigliana creek case study is not limited to the geophysical measurements described in Subsections 3.2 and 3.3. In fact, some auxiliary geophysical datasets are available to better understand the structures of this site. More in

Table 1
Summary of the dates of the seasonal ERT and DTS measurements between 2013 and 2015. For the detailed times of the short-term monitoring, please refer to Table 2. The DTS acquisitions on July 24, 2015 and August 27, 2015 did not take place due to an instrument failure. The December 11, 2015 ERT measurement was not performed because of the climatic conditions (i.e. frozen soil covered in snow).

Summary of seasonal geophysical monitoring	
Auxiliary geophysical acquisitions	
2011: GPR	2013: ERT
6th October	30th July
Seasonal geophysical monitoring	
2013	
ERT	DTS
2nd July	Not installed yet
30th July	
27th August	
24th October	
17th December	
2015	
ERT	DTS
29th April	29th April
19th May	19th May
17th June	17th June
30th June–1st July (short term monitoring)	30th June–1st July (short term monitoring)
24th July	6th November
27th August	11th December
6th November	

Table 2
Summary of times (CET) of the 2015 ERT and DTS short term monitoring performed between June 30 and July 1.

Short-term monitoring dates and times	
June 30, 2015	
ERT	DTS
9:00 am	9:25 am
10:00 am	10:30 am
11:00 am	11:40 am
12:00 pm	12:30 pm
2:00 pm	2:30 pm
4:00 pm	4:30 pm
6:00 pm	6:30 pm
10:40 pm	7:15 pm
	10:50 pm
July 1, 2015	
ERT	DTS
3:00 am	3:25 am
8:00 am	8:10 am
9:00 am	9:30 am
11:00 am	11:00 am
1:00 pm	12:55 pm
3:00 pm	3:00 pm
5:00 pm	16:55 pm

detail, such investigations include ground penetrating radar (GPR) and surface ERT surveys that were part of previous campaigns, having the goal of defining the larger scale structure of the river bottom.

The GPR surveys took place in October 2011 using a PulseEKKO Pro instrument (Sensor and Software Inc.) with 50 MHz antennae in a common offset acquisition mode (i.e. the distance between the two antennas – transmitter and receiver – is constant throughout the whole acquisition). The survey lines were run to understand the overall structure of the valley bottom. Fig. 3b shows one such line, taken perpendicular to the creek, and covering the right embankment from the river bank to the beginning of the slope. The radargram shown in Fig. 3 is compared against the ERT static resistivity distribution obtained in July 2013 and a cross-section of the valley bottom (Dal Piaz et al., 2007). The two geophysical surveys concur in indicating that a solid bedrock is present around 10 m below the riverbed, becoming shallower while moving toward the valley sides, where it outcrops. This evidence defines the thickness of the alluvial cover in the area of interest and agrees with the geological information available (see Section 2), which also describes the strong scattering characterizing the radargram.

On July 30, 2015, an auxiliary ERT profile was collected placing a waterproof multicore cable (equipped with 48 graphite electrodes with 1 m spacing) longitudinally on the riverbed, a few meters upstream of the bridge (and the ERT and DTS installations). The acquisition scheme was a dipole-dipole skip zero. The reciprocal error threshold was set equal to 10%, in agreement with the other ERT acquisitions. The resulting 2D section (Fig. 4) shows the presence of a very low resistive domain along the whole survey line, located in the shallow subriverbed, while the rest of the resistivity section is characterized by two subdomains with depth, one with higher mean resistivity (between 2500 and 5000 Ωm, or more) and a deeper one having lower conductivity.

3.5. Hydrological modeling and application to the 2015 short-term monitoring

In order to take full advantage of the information content in the datasets at our disposal, we developed a three-dimensional finite element hydrological model representing the hyporheic zone of the Vermigliana creek, with a focus on the application to the short-term monitoring performed in 2015. To this end, we have utilized FEMWATER (version 3.0.5, Lin et al., 1996), a finite element solver of Richards' three-dimensional equation in variably saturated media. More in detail, the modeling phase is made of two distinct parts:

1) A flow model, aimed at showing how the pressure head distribution varies over time and space as a consequence of the fluctuating water level of the Vermigliana creek;
2) A solute transport model, that predicts the variations of the electrical resistivity of water in the modelled domain. Its results are compared with the ERT absolute and the time-lapse ERT inversions, and with the DTS profiles.

3.5.1. Mesh set-up

The three-dimensional mesh (Fig. 5) is composed of 22,464 nodes and 40,020 triangular prismatic elements, subdivided into 15 layers whose thickness increases with depth. The geometry of the mesh top

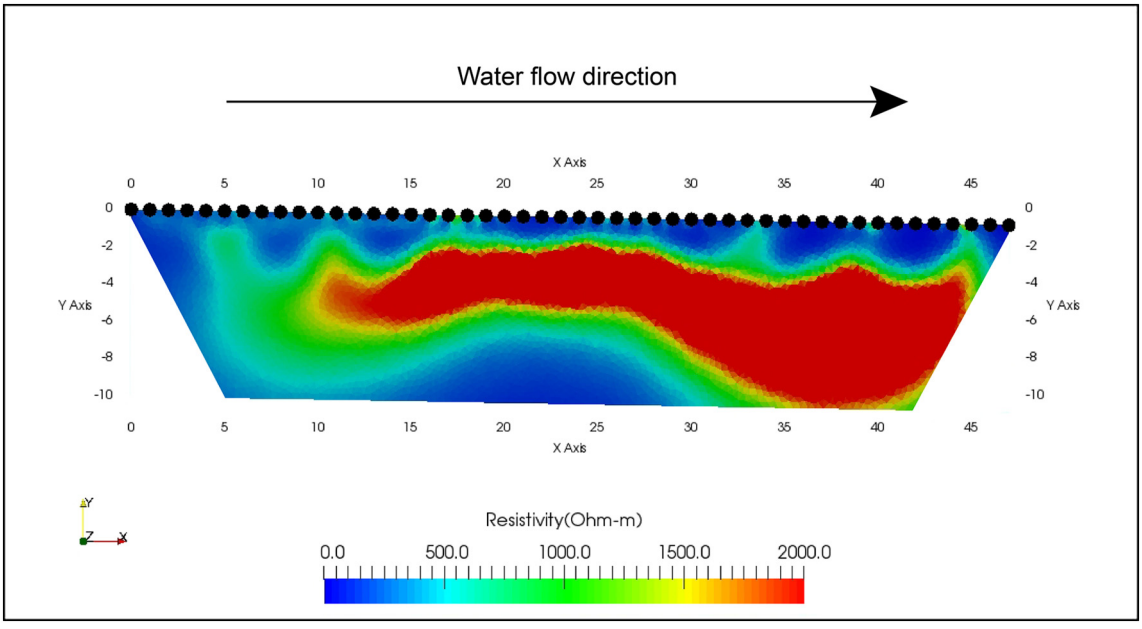

Fig. 4. Resistivity cross-section resulting from the static inversion of the auxiliary ERT acquisition performed on July 30, 2015. The black dots represent the 48 electrodes embedded in the multicore cable placed on the riverbed, parallel to the water flow direction.

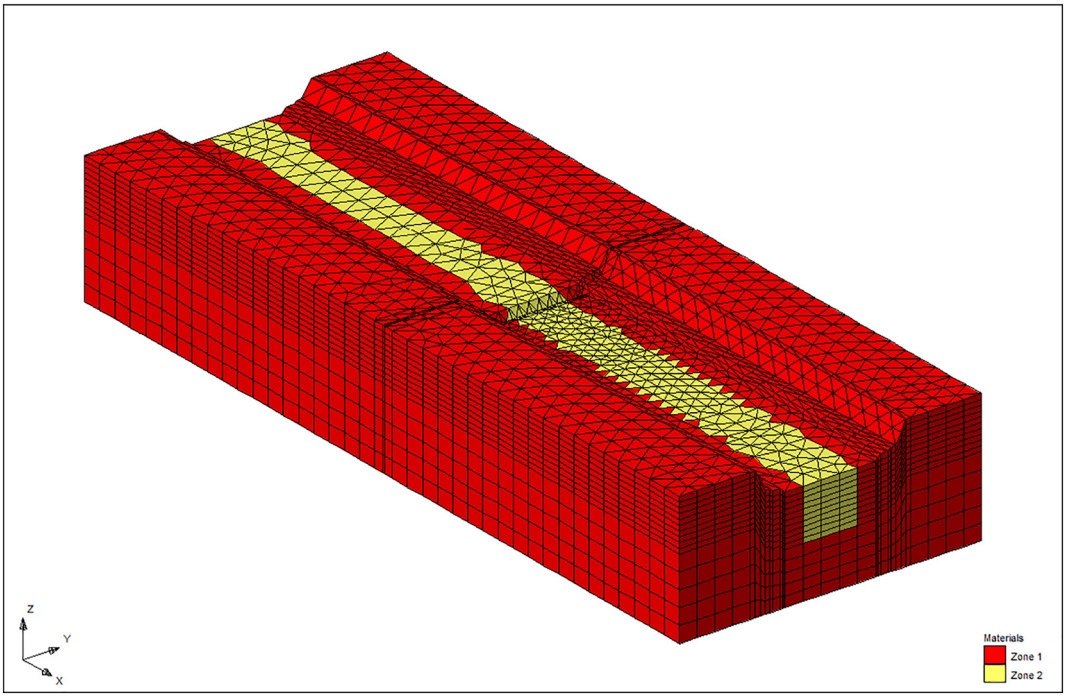

Fig. 5. 3D mesh created for modeling flow and solute transport processes in the Vermigliana Creek site. The mesh is composed of 22,464 nodes, 40,020 triangular prismatic elements and the elements "Zone 1" and "Zone 2" are highlighted.

surface is designed according to the results of a topographic campaign performed in 2016. The surface consists of a sloping river bottom (average slope equal to 1.8%) with the left and right embankments and the bottom pit located at a distance in the *x* direction between 37.5 m and 38.75 m from the origin upstream. The mesh horizontal size is 75.0 m long, 30.0 m wide, and, at every section, its depth in correspondence of the thalweg is equal to 10.0 m, except for the pit section, where the vertical thickness is reduced (i.e. <10.0 m) in order to maintain the mesh bottom flat. In other words, the thickness of the whole mesh is constant along the *x* direction, considering an irregular topography and a flat, sloping bottom, while the thickness of the layers varies within the different vertical sections, since the number of layers is fixed to 15 throughout the mesh. The elements of the mesh are subdivided into two zones: (i) "Zone 1" corresponding to the clastic material filling

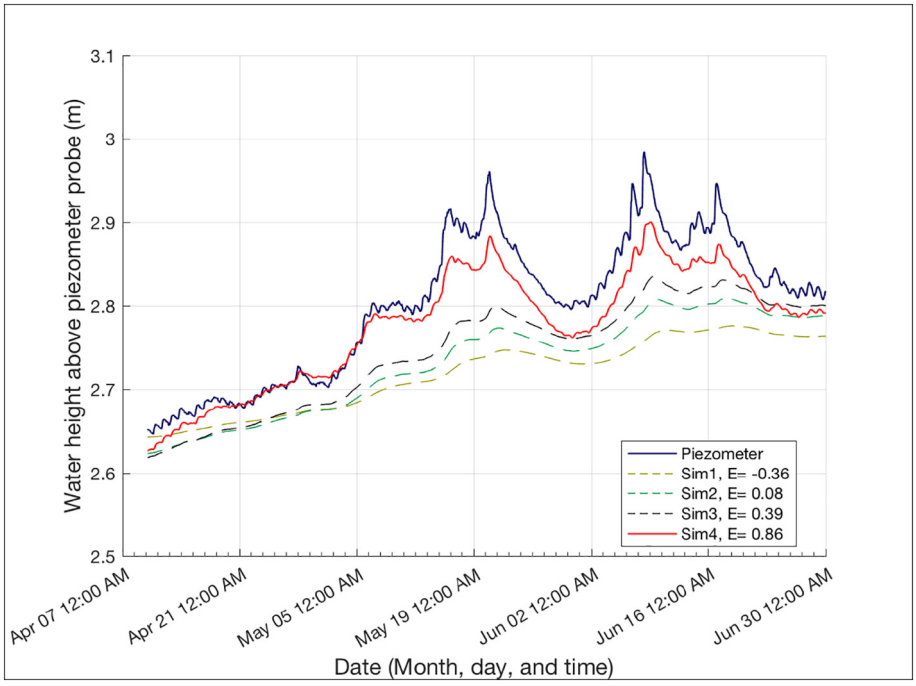

Fig. 6. Flow model calibration results referred to the period April–July 2015. The blue solid line is the water height above the piezometer prove, while the other curves represent different flow simulations with the corresponding Nash-Sutcliffe model efficiency coefficient (E; Nash and Sutcliffe, 1970). The red solid line represents the chosen calibration curve. (For interpretation of the references to colour in this figure legend, the reader is referred to the web version of this article.)

Table 3
Material properties used for the Vermigliana Creek flow model calibration. The parameters that give the chosen calibration curve are in italic (Simulation 4). In all simulations, the residual moisture content values come from the parameters available in FEMWATER for the linear front retention curves, as well as the porosity values in Simulations 1 and 2. In all the other simulations, porosity values and saturated hydraulic conductivity (K_s) come from Terzaghi et al. (1996).

		Material	Saturated hydraulic conductivity	Porosity	Residual moisture content
Simulation 1	Zone 1	Loam	5.0e−7 m/s	0.43	0.078
	Zone 2	Clay loam	5.0e−8 m/s	0.41	0.095
Simulation 2	Zone 1	Sandy loam	1.0e−6 m/s	0.41	0.065
	Zone 2	Sandy clay	1.0e−8 m/s	0.38	0.1
Simulation 3	Zone 1	Loam	1.0e−6 m/s	0.30	0.078
	Zone 2	Clay loam	1.0e−8 m/s	0.25	0.095
Simulation 4	*Zone 1*	*Loam*	*2.0e−6 m/s*	*0.16*	*0.078*
	Zone 2	*Clay loam*	*3.0e−8 m/s*	*0.15*	*0.095*

the Val di Sole and (ii) "Zone 2" representing the low resistivity domain shown by the absolute ERT inversions in the sub-riverbed (see Subsection 4.1.1.1).

3.5.2. Flow model set-up and calibration

The flow modeling covers the time period from January 1, 2015 12:00 am to July 1, 2015 11:59 pm. We applied a no-flow Neumann boundary condition at the mesh bottom, at the mesh right and left boundaries (with respect to the flow of the Vermigliana water, which takes place along the x direction from $x = 0.0$ m to $x = 75.0$ m), and on the top surface with the exception of the riverbed, where the varying water level is imposed as a transient Dirichlet boundary condition corresponding to the changing river stage. On the upstream and downstream mesh boundaries (i.e. at $x = 0.0$ m and $x = 75.0$ m), we applied a constant total head Dirichlet boundary condition determined on the basis of the mean water table depth measured during the observation time interval by the piezometer probe. The initial condition consists of a pressure head distribution obtained assuming a horizontal water table, whose depth is, again, the mean water table depth. The simulation time is equal to 182 days (i.e. 15,724,800 s) while the time step is constant and equal to 5 min (i.e. 300 s). Note that most of the simulation time is a warm-up period necessary to reproduce the conditions at the start of the short-term monitoring period on June 30, 2015, 9:00 a.m. Precipitation is neglected.

The model calibration was performed comparing the fluctuation of the water table measured by the piezometer probe with the model output in correspondence of the position of the piezometer itself. The calibration was performed simply on a trial-and-error basis. The result is shown in Fig. 6 (which shows only the period that ranges from April 10 to July 1, 2015) and allows us to determine the most suitable set of hydrological parameters for the two materials, corresponding to the "Zone 1"–"Zone 2" element mesh subdivision. These parameters, summarised in Table 3, describe the two materials both in saturated and unsaturated conditions. In the latter case, in particular, we adopted simple "linear front" water retention curves, which consist in a linear interpolation between the maximum and minimum values indicated for each parameter (e.g. maximum and minimum moisture content). This decision is due to two reasons: (i) the limited information available for the retention curves in the domain and at the scale of interest, and, more important (ii) the subdomain we are actually interested in (i.e. the sub-riverbed under the Vermigliana creek) is always in saturated conditions, while the water retention parameters influence the model solution only in correspondence of the shallower part of the embankments. More in detail, Fig. 6 shows a few calibration curves, which result from the application of different sets of parameters to the flow model. Although each of these sets provides an adequate solution to the transport model (see the following Subsection 4.2 where an explanation is given for this apparent paradox), it is clear that only one of the shown modelled solutions corresponds to a valid calibration of the flow model. Proceeding by a simple trial-and-error, the best set of parameters is therefore chosen on the basis of the Nash-Sutcliffe model efficiency coefficient (Nash and Sutcliffe, 1970):

$$E = 1 - \frac{\sum_{t=1}^{T} \left(Q_m^t - Q_o^t\right)^2}{\sum_{t=1}^{T} \left(Q_o^t - \overline{Q}_o\right)^2} \quad (1)$$

where Q_o^t is the observed discharge at time t, $\overline{Q}_o$ is the mean observed discharge over the whole observation time, and Q_m^t is the modelled discharge at time t (in this case, however, we considered the water height above the piezometer probe as defining variable). If $E = 1$, the model perfectly describes the observed data, hence we adopted the set of parameters with E closest to 1 (i.e. Simulation 4, $E = 0.86$). Note though that, in the time interval considered, the corresponding modelled curve always underestimates the real data. Nevertheless, we considered this as the best solution (among those available) since this difference is mostly due to the fact that we do not consider precipitation in the flow model. The set parameters thus chosen describe a glacial till in accordance with Terzaghi et al., 1996.

3.5.3. Solute transport model set-up

The solute transport model was developed for a shorter time range, from May 27, 2015 at 4:00 pm to July 1, 2015 at 11:59 pm, and is based on the pressure head field computed by the calibrated flow model described in Section 3.5.2. Thus, the simulation time is equal to 35 days and 8 h (i.e. 3,052,800 s), the time step is constant and equal to 5 min (i.e. 300 s), and the three-dimensional mesh is again the one represented in Fig. 5. In addition to the parameters indicated in Table 3, the solute transport model requires further specifications regarding the material properties. In particular, information about bulk density, tortuosity, longitudinal and lateral dispersivities, and the molecular diffusion coefficient are necessary. The adopted values are summarised in Table 4. Note that the influence of these parameters is relatively small in the considered context, where the forcing condition of the river is overwhelming and dictates the transport dynamics over short distances, where advection is the controlling mechanism.

The Dirichlet boundary condition consists in the transient concentration of total dissolved solids (TDS) in the water of the river. This

Table 4
Material properties used in the solute transport model to describe Zone 1 and Zone 2. The bulk density values come from Terzaghi et al. (1996), while the molecular self-diffusion coefficient of water is provided by Holz et al. (2000). The longitudinal and lateral dispersivity are assumed, as well as the tortuosity.

	Material	Bulk density	Tortuosity	Longitudinal dispersivity	Lateral dispersivity	Molecular diffusion coefficient
Zone 1	Loam	1800.0 kg/m^3	1.0	20.0 m	5.0 m	2.299e−9 m^2/s
Zone 2	Clay loam	2000.0 kg/m^3	1.0	5.0 m	1.0 m	2.299e−9 m^2/s

value is obtained from the actual resistivity of the river water (measured by the river probe, see Section 3), conveniently transformed in the corresponding TDS concentration according to Eq. (2) (Hem, 1985)

$$S = KA \tag{2}$$

where S is the TDS concentration (mg/l), K is the specific electrical conductivity (μS/cm), and A is a constant that ranges, in most cases, between 0.54 and 0.96 (here we assumed $A = 0.6$).

3.5.4. Solute transport model post-processing

Once the solute transport model is run, the resulting concentration distribution in the whole domain is then turned backward into the corresponding water electrical resistivity, according to Eq. (2). The values thus obtained allow us to compute the corresponding bulk resistivity distribution, which can be compared with the results of the absolute ERT inversion. This is possible thanks to two petrophysical relationships:

1. Archie's law (Archie, 1942):

$$\rho_b = \frac{a}{\phi^m S_w^n}\rho_w = F\rho_w \tag{3}$$

where ρ_b is the bulk electrical resistivity, ϕ is the porosity, S_w is the water saturation, ρ_w is the electrical resistivity of the water filling the pores, a, m, and n are the tortuosity parameter, the cementation exponent, and the saturation exponent, respectively, and F is the formation factor. Since we are focusing only on the sub-riverbed, we have that S_w is equal to 1 (i.e. the domain is water saturated) and so the value of n does not need to be determined. Finally, we put $a = 1$ and $m = 1.4$ as they led to the best match between the ERT static data and the bulk resistivity thus computed from the solute model outcome (these values agree with literature examples, see e.g. Lesmes and Friedman, 2005);

2. Waxman and Smits (1968) corrected Archie's law (Eq. (3)) in order to consider also the solid matrix surface conductivity σ_s as:

$$\sigma_b = \frac{\sigma_w}{F} + \sigma_s \tag{4}$$

where σ_w is the water electrical conductivity ($\sigma_w = 1/\rho_w$). In particular, Waxman and Smits (1968) propose that

$$\sigma_s = \frac{BQ_v}{F} \tag{5}$$

where Q_v is the volume concentration of clay exchange cations (meq/cm^3) and B is the equivalent conductance of the clay counterions. Moreover, Sen et al. (1988) defined B as a function of m and σ_w:

$$B = \frac{1.93m}{1 + \frac{0.7}{\sigma_w}} \tag{6}$$

In this work, we put $m = 1.2$ and $Q_v = 1.8$ on the basis, once again, of the comparison between the static results of the ERT analysis and the bulk resistivity thus computed form the outcome of the solute transport model (see e.g. Lesmes and Friedman, 2005; Monego et al., 2010);

We decided to consider these two petrophysical relationships in order to take into account the different electrical properties of the two subsoil materials. In fact, we suppose that the low resistivity domain in the ERT absolute images (see Fig. 7 and Subsection 4.1.1.1 for the description) is due to a higher fine material fraction (see Section 5 for a discussion). Therefore, Archie's law cannot be applied in this region of the hyporheic zone, thus requiring a more appropriate petrophysical model (i.e. Waxman and Smits, 1968).

Determining the bulk resistivity allows also computing the resistivity percentage change ($\Delta\rho$), over time, with respect to a background condition, as:

$$\Delta\rho_b = \frac{(\rho_{b,t} - \rho_{b,0})}{|\rho_{b,0}|}100(\%) \tag{7}$$

where $\rho_{b,\,t}$ is the bulk resistivity at the different times t and $\rho_{b,\,0}$ is the bulk resistivity at $t = 0$, i.e. the background condition. Eq. (7) is applied to each node of the mesh and the $\Delta\rho_b$ distribution thus obtained is compared with the ERT time-lapse inversion.

4. Results

4.1. Geophysical monitoring results

4.1.1. ERT results

Even if the time-lapse geophysical characterization of the Vermigliana case study comprises several years of acquisitions between spring and early autumn (Table 1), the most interesting results come from the analysis of the data collected during the 2015 campaign, since also a complete dataset of water level, electrical conductivity and temperature (both for the river and the local aquifer) is available (see Section 3). In fact, in order to completely describe the domain of interest, the geophysical data need to be integrated with this additional information.

4.1.1.1. ERT static characterization. The ERT static characterization along the Vermigliana Creek cross-section shows the presence of two main

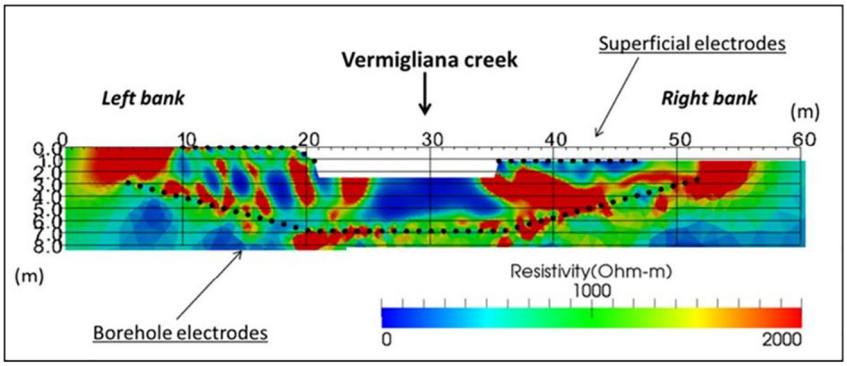

Fig. 7. An example of static ERT cross-section that shows the state of the domain at the measurement time (on April 29, 2015, background acquisition). The 2D section is characterized by: i) a low resistivity domain within the sub-riverbed (probably due to a high fine material fraction); ii) a complex domain in terms of electrical resistivity values in correspondence of left and right banks (most likely due to the presence of boulders, in agreement with the material filling the Val di Sole).

domains (Fig. 7): (i) the sub-riverbed, characterized by relatively low electrical resistivity values, probably related to the presence of deposits with a high clay/silt fraction likely put in place by the creek itself – note that the river was straightened in the recent few decades, and is now occupying a bed different from the original braided one; (ii) the left and right banks of the Vermigliana creek, characterized by complex subdomains, that are compatible with the presence of heterogeneous deposits (glacial till) in this region. More in detail, the left bank has a slightly lower average electrical resistivity compared to the right bank, due to the local effect of the two small lakes (see Section 5 for a discussion).

4.1.1.2. ERT seasonal and short-term monitoring. The 2015 ERT seasonal time-lapse results are reported in Fig. 8. In particular, the computed resistivity variation is expressed in terms of percentage: a value of 100% indicates that the value is identical to that of the background, while higher values (i.e. >100%) display in increase in resistivity and lower values (i.e. <100%) denote a decrease in resistivity over time.

The time-lapse inversion of such dataset, obtained according to the ratio approach of Daily et al. (1992), shows an increase in electrical resistivity between May and August 2015 (Fig. 8, from a to d) inside the hyporheic zone, which is then followed by a decrease in this parameter during November 2015 (Fig. 8e). The left bank shows an average decrease in electrical resistivity from May to August 2015 and then an increase during November 2015. The right bank shows, instead, a more complex behavior, which will be object of further investigations in the future.

On the other hand, the short-term monitoring focuses on the fast dynamics of the sub-riverbed, given the higher frequency of the measurements. From this dataset it is apparent how a frequent time-lapse acquisition is necessary to track the surface water-groundwater interactions. Fig. 9 shows the results of this monitoring in terms of resistivity variations. For brevity, only a selection of the most relevant times is presented. Fig. 9a shows that the variations between 11:00 am and 9:00 am on June 30 (where 9:00 am, June 30 is the background acquisition, Fig. 7) is too small to be computed: the first time with a detectable resistivity variation is 4:00 pm on July 30. Fig. 9b (6:00 pm vs 9:00 am, June, 30) shows a decrease in resistivity in the sub-riverbed. Then, in Fig. 9c, the whole domain is characterized by very small variations and finally, in Fig. 9d (1:00 pm – July 1 vs 9:00 am – June 30) the resistivity decreases again. The resistivity increment in correspondence of the surface electrodes is due to the strong evapotranspiration and the lack of precipitation that took place during those hours.

4.1.2. DTS results: seasonal and short-term monitoring

The temperature information provided by the 2015 DTS seasonal monitoring describes the site's dynamic behavior. In particular, a heating trend was recorded between April and July 2015 (Figs. 10 and 11) and a cooling trend from November to December 2015 (Fig. 10). Four different subdomains may be identified in the DTS profile: (i) the sub-riverbed zone, which shows a rather complex behavior during the hot season, with two minimum peaks probably related to the infiltration of new (cold) glacial water, and a smoother trend during cold periods; (ii) the left and (iii) right banks, which are characterized by different average temperatures, likely because of the influence of the water coming from the two small ponds (Fig. 1), as described also in the ERT results (Subsection 4.1.1.1); (iv) the coiled portion of the optical fiber, which represents a segment of the cable coiled at a depth of 0.5 m below ground level, thus representing a reference value. The 2015 DTS seasonal dataset lacks the acquisition of July, 24 and August, 27 because of an instrumentation failure, but it includes also two measurements performed when the field site was already covered in snow, i.e. November, 6 and December, 11 (Table 1). As shown in Fig. 10, these temperature profiles present different trends with respect to what happens during the hottest months: not only the average temperature is lower, but it also decreases between November and December, in accordance with the climatic features of the site (Section 2). Once again, a difference arises between the spatial sectors, in particular between the sub-riverbed/right bank and the left bank. The latter, in fact, is colder with respect to the two other parts.

A quantitative time-lapse analysis confirms the qualitative description above. In fact, from April to July the mean temperature increases of 4.3 °C. However, this temperature variation is not constant along the whole cable, since the two banks warm up in two slightly different ways: the mean temperature increase on the left bank, between April and July, is equal to 4.8 °C, while on the right bank it is equal to 4.4 °C. Furthermore, this is also confirmed by the temperature variation computed for each sampling point. Therefore, we can assume that such temperature variation over time is instrument independent, but also we can hypothesize that the left and right riverbanks behave in two different ways, or, more likely, that are subject to different phenomena.

The DTS short-term monitoring (Table 2, Fig. 12b, and Video 1) exhibits the quick dynamics of the hyporheic zone temperature variations. It is important to note the temperature variation that takes place over time. On average, the temperature is constant between 9:25 am and 12:30 pm on June 30, then it increases until 10:50 pm, it decreases again until 11:00 am on July 1 and finally increases again until the end of the monitoring period. If compared to the information provided by the river probe (Fig. 12a), this "sinusoidal" trend resembles the one of the river water, although with a small (expected) time delay.

4.2. Solute transport model results

The results of the transport model in terms of resistivity variations are shown in Fig. 13, where they are compared with the ERT time-lapse results (Subsection 4.1.1.2) and the temperature trend

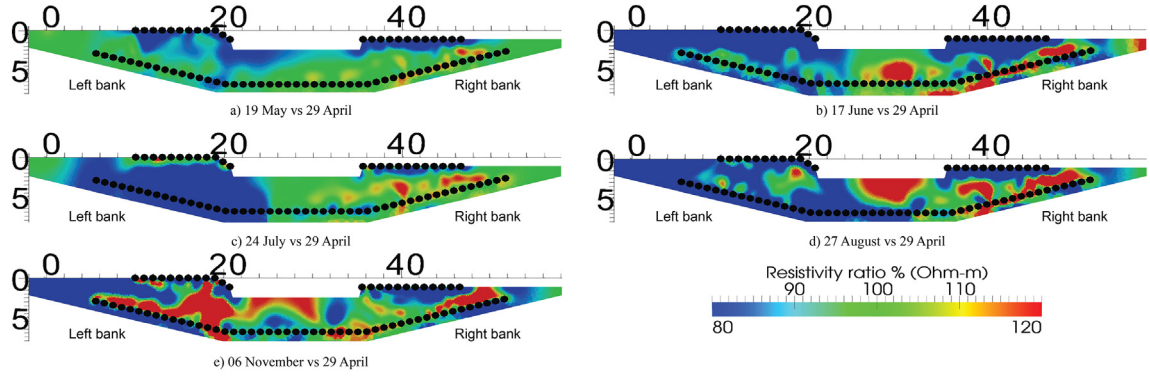

Fig. 8. a–e) 2015 ERT seasonal monitoring of the Vermigliana creek, expressed in terms of resistivity variation with respect to the background acquisition (April 29, 2015). The value "100%" indicates no changes in electrical resistivity with respect to background survey, higher values imply an increase in electrical resistivity, while lower values are related to a decrease. The black dots represent both surface and borehole electrodes. Distances are expressed in meters.

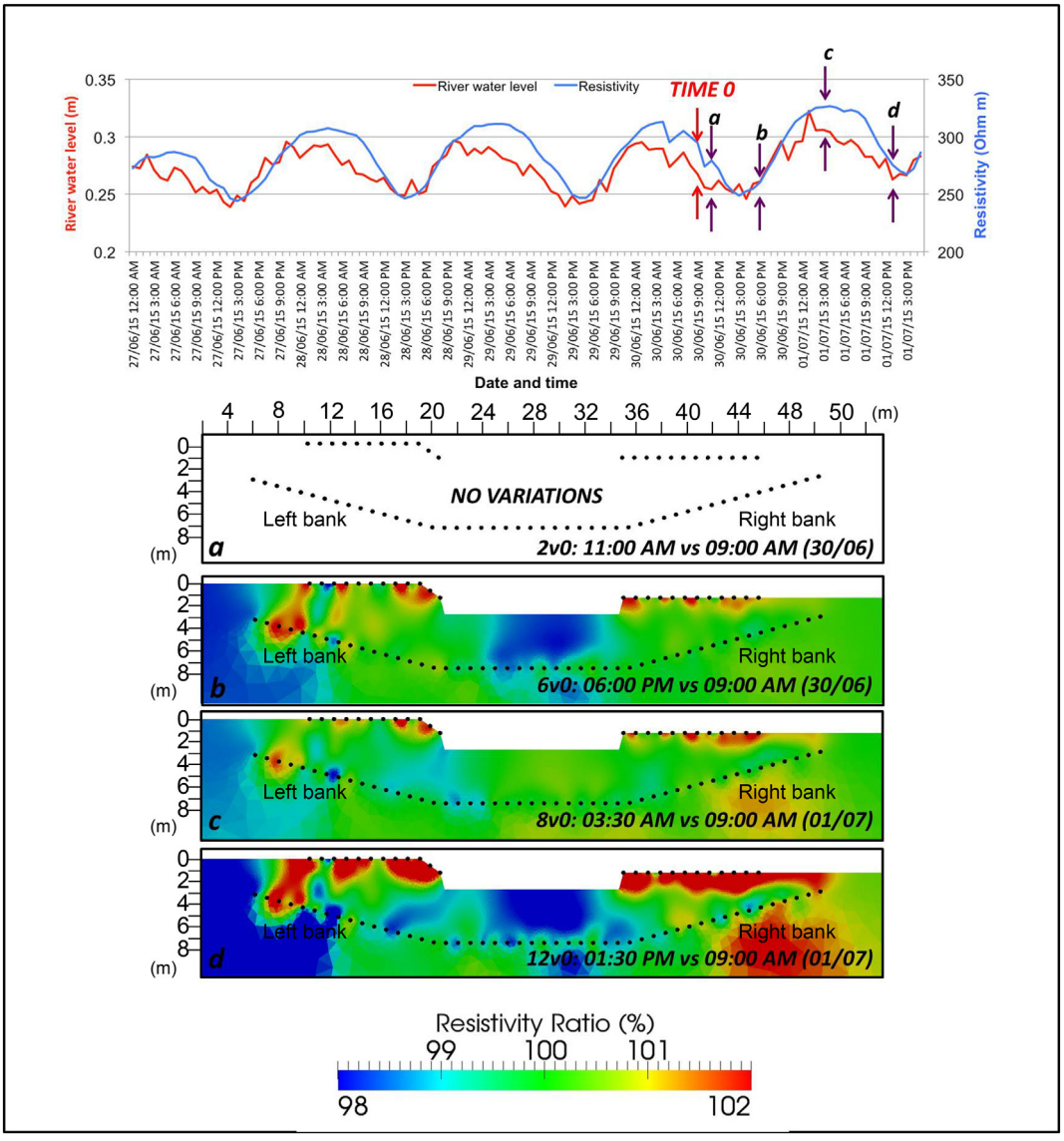

Fig. 9. Comparison between river data (water level and water resistivity) and a selection of 2015 ERT short-term monitoring results (a–d), expressed as resistivity variations. In the river water graph, "a, b, c, d" and "Time 0" indicate the correspondence between the ERT acquisition times and the hydrological information. Regarding the ERT sections, a value of "100%" indicates no changes in electrical resistivity with respect to the background survey (conducted on June 30, 2015, at 9:00 am). Higher values imply an increase in electrical resistivity, while lower values are related to a decrease. The black dots represent both surface and borehole electrodes.

highlighted by the DTS (Section 4.1.2). More in detail, to simplify the comparison between the two resistivity datasets, we consider only the central 8 m of the sub-riverbed, till a depth of 5 m, in order to: (i) remove any effect of the creek's banks; and (ii) refer to the domain investigated by the ERT acquisitions (i.e. the borehole electrodes are located 5 m under the riverbed, see Fig. 2). The resistivity values in this subdomain are then averaged, so as to assign a single mean bulk resistivity variation value to each time. Even if this may seem a strong simplification, it allows a better representation (and an easier comparison) of the variation trends identified by the two methods.

The DTS temperature values in the sub-riverbed are averaged at each time-step as well, in conformity with the ERT and transport model post-processing. In this case, however, we consider also a further precaution, distinguishing between the left and right parts: in fact, they not only show a slightly different behavior in correspondence of the relative peak (the left part relative maximum is at time 10:50 pm on June 30, while on the right side the relative maximum is at 3:35 am on July 1), but also have different mean temperatures, with the left section being hotter than the right segment.

5. Discussion

5.1. Sub-riverbed

The results provided by the geophysical measurements give some interesting insights into the areas surrounding the Vermigliana creek riverbed. A first important information comes from the ERT static inversion (Fig. 7), where a very low resistivity area (less the 200 Ωm, on average) characterizes the sub-riverbed. At a first glance, the presence of such domain may be justified by the seepage process, which allows the sub-riverbed saturation with the consequent overall resistivity modification (as expected, according to Archie, 1942). Nevertheless, if we focus on the resistivity values instead, a discrepancy arises: an average resistivity lower than 200 Ωm is incompatible with the values characterizing both deposits and waters of the Vermigliana creek, whose resistivity values are in the range of 1000 Ωm (see the right and left embankments, Fig. 7) and 100 Ωm (graph in Fig. 9) respectively. In order to explain the features of this domain, whose existence in the sub-riverbed is also confirmed by the longitudinal ERT survey on the riverbed (Fig. 4),

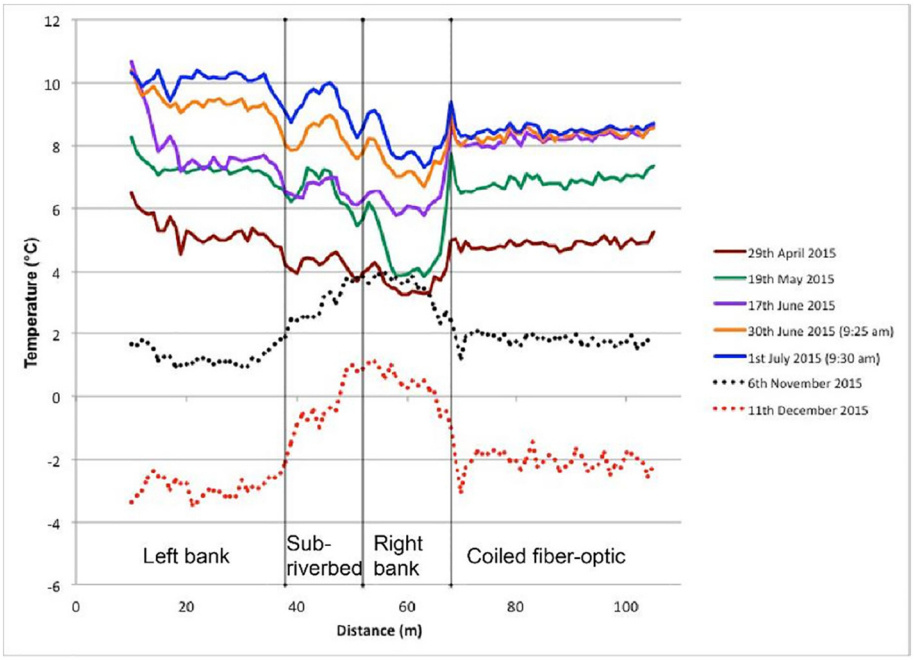

Fig. 10. 2015 DTS seasonal monitoring. Between April and July 2015 an average increase in temperature takes place, while from November to December 2015 an average decrease occurs, as well as a temperature trend inversion. Four subdomains, with different characteristics, can be identified for each survey time: left bank, hyporheic zone, right bank, and coiled fiber-optic. Note the different behavior between left bank and right bank in terms of temperature, but also the effect of infiltration of new cold glacial water in the hyporheic zone.

we hypothesize the presence of a high clay/silt fraction coming from the glacial moraines and transported by the creek itself, which not only increases the electrical conductivity in the sub–riverbed, but also reduces its hydraulic conductivity. Filtering from the stream into the man-made new riverbed is likely to have caused partial clogging of the original sediments with this fine material. This hypothesis agrees with the results of the short-term ERT time-lapse monitoring (Fig. 9a, b, c, d), where the resistivity variations in the sub-riverbed, despite taking place on an hourly basis, are slightly mitigated (and have a lower amplitude) with respect to what is happening in the river. As a matter of fact, figures show that the resistivity of the river water, with respect to that at Time 0, decreased by 5% at "Time a", by 11% at "Time b", increased by 10% at "Time c" and finally decreased by 3% at "Time d". Even though the ERT time-lapse cross-sections show the same pattern, the magnitude of the variation is slightly lower, as it ranges from a 2% decrease to a 2% increase (Fig. 9).

The effects of the infiltration of new glacial water can be recognized also in the seasonal DTS time-lapse monitoring. Even if the mean temperature increases (as a consequence of the climatic conditions of the site), an active underflow dynamic within the sub-riverbed is underlined by the presence of two minima in the temperature trend, which may represent two preferential seepage pathways (Figs. 10 and 11). Furthermore, a comparison between the seasonal DTS and ERT monitoring show an agreement between the two results, where the

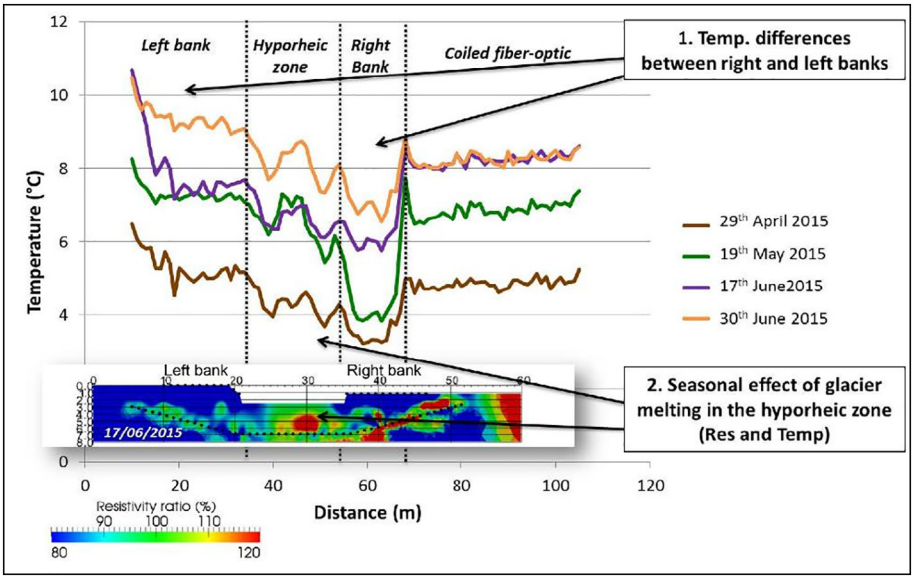

Fig. 11. Comparison between seasonal DTS and ERT time-lapse data collected during Season 2015. Note the seasonal effect of glacier melting within the sub-riverbed, both in terms of temperature (T, expressed in °C) and electrical resistivity variation (expressed in %). The value "100%" indicates no changes in electrical resistivity with respect to background survey (in this case conducted on 29th April 2015); higher values imply an increase in electrical resistivity.

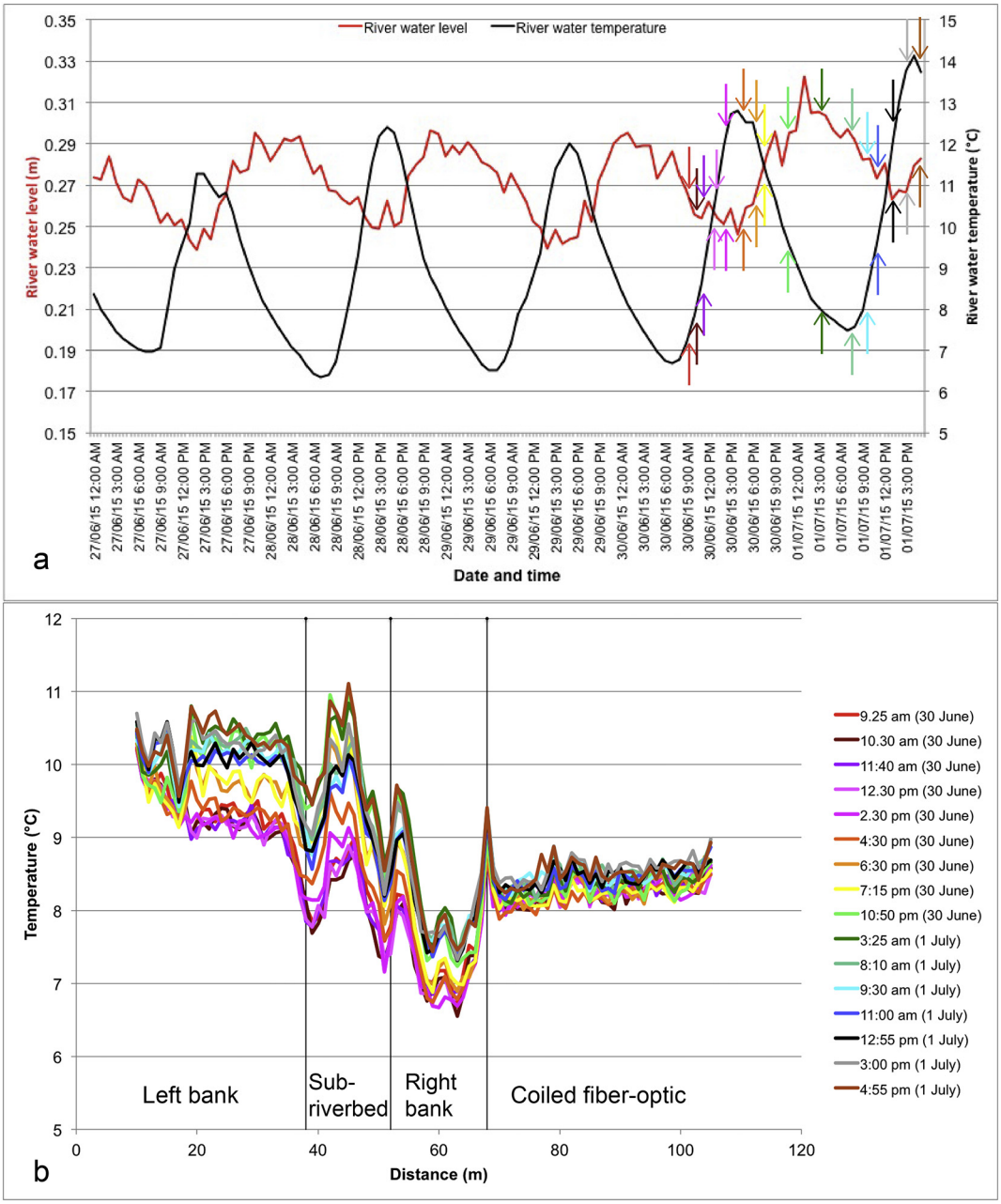

Fig. 12. Comparison between a) river data (water level and temperature) and b) DTS temperature profiles collected during the short-term monitoring (June 30–July 1, 2015). For a better comprehension of the temperature trend highlighted by the DTS monitoring, please refer to Video 1.

infiltration of new glacial water, despite the slightly higher temperature, leads to a decrease in resistivity given the lower TDS concentration. Therefore, the resistivity ratio and temperature changes, caused by the high resistivity glacial outflows water, are much likely linked to the river flow rate.

Finally, the effects of the infiltration of new water in the sub-riverbed are particularly clear in the short-term DTS time-lapse monitoring. In detail, the temperature trend along each profile has the same properties of those included in the seasonal monitoring (i.e. two minima in the sub-riverbed). However, given the higher time resolution, we can also easily observe a sinusoidal trend comparable to that of the creek water, though slightly delayed (Fig. 12 and Video 1). The amplitude of this variation, even if smaller than what is highlighted by the river probe, is still rather large and agrees with the description of temperature trends in the sub-riverbed of losing steams provided e.g. by Constantz (2008).

5.2. Riparian zones

Another feature on which attention shall be focused is the difference between the right and left embankments. This contrast arises in all the geophysical time-lapse monitoring, with particular evidence in the seasonal ERT (Fig. 8) and in the seasonal and short-term DTS results (Figs. 10 and 12). The cause of this dissimilar behavior should be sought in the presence, on the left bank, of the emissary of the two ponds upstream (Fig. 1). The water of this small brook has both a higher temperature and a higher TDS concentration with respect to the Vermigliana Creek water (given its higher residence time in the shallow lakes), so its infiltration explains the variations displayed by both techniques: (i) the left bank has always, on average, a higher temperature with respect to the right bank (where no evidence of superficial water flow is present); and (ii) higher TDS concentrations and higher temperatures reduce the electrical resistivity of the water, whose infiltration reduces,

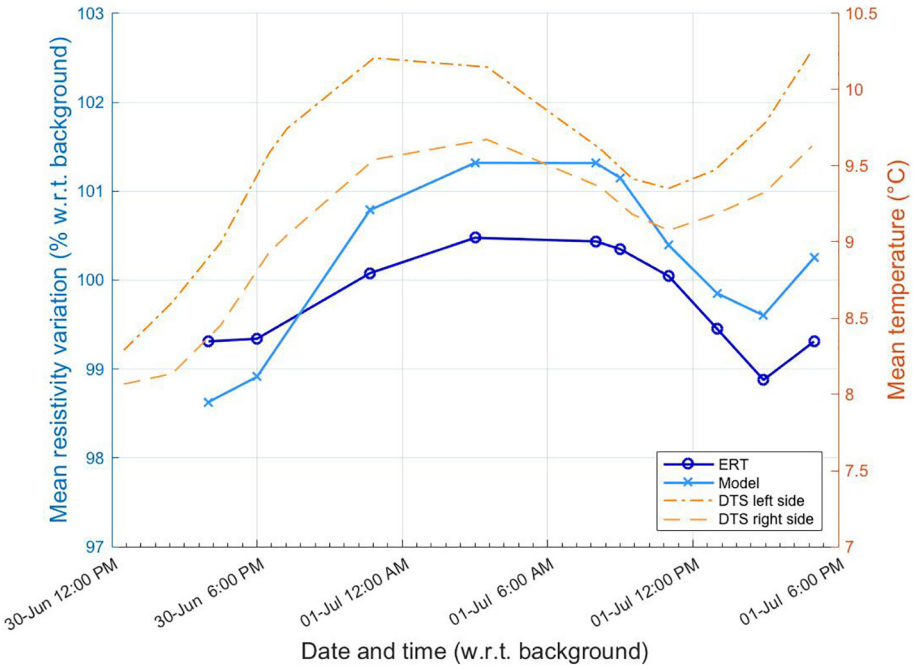

Fig. 13. Comparison between ERT time-lapse monitoring, solute transport model, and DTS time-lapse monitoring (with the dataset separated in central-right and central-left sides). All datasets refer only to the sub-riverbed zone and are averaged to obtain a single value for each time. The DTS dataset is split in two parts to show the influence of the emissary of the two small lakes, which slightly increases the temperature on the left side.

in turn, the bulk resistivity over time (Fig. 8a–c). From the end of August on, the average temperature starts decreasing again (Section 2), thus leading to an increase in resistivity (Fig. 8d–e). Unfortunately, this decrease in temperature has not been measured by means of DTS because of a system failure.

5.3. Hydrological model

The goal of the hydrological modeling in this work is to demonstrate how powerful a combination of geophysical and hydrological information is in order to understand the processes occurring in the hyporheic zone. The ERT datasets are exploited in two different ways. As described in Section 3, we took advantage of a combination of the information provided. In fact, the ERT static inversion results are used to identify the two main zones in the model mesh, but their hydrological parameters are chosen on the basis of a comparison between the similarity with the water table height measured by the piezometer probe and the results of the solute transport model (i.e. whether they agree or not with ERT time-lapse outcome).

In the latter case, the phase of the resistivity variation trend agrees with the ERT time-lapse results (Fig. 13) since both curves have their maximum at 3:00 am on 1st July. The amplitude, however, is slightly different, as the ERT time-lapse shows a smoother trend. This may be given by small variations taking placing in the sub-riverbed but, most of all, it is also related the type of inversion performed (i.e. Occam's approach, see Section 3.2.1), which is based on a smoothness constraint aimed at providing a stable solution.

Even if in this work we did not develop a heat transport model, we used the temperature data from DTS as an auxiliary piece of information to strengthen the results of the ERT monitoring coupled with the transport model. Thus, Fig. 13 includes also the temperature data from DTS measurements in the sub-riverbed because, under some circumstances, heat transport can be described by the same equations of the solute transport (the Advection Dispersion Equation or ADE). More specifically, for this to be true, the heat capacity of the solid material has to be negligible with respect to that of the water, and heat conduction must be negligible with respect to heat advection. In Fig. 13, the comparison between the DTS measured data and the modelled ERT variations shows that, in our case, the trend is the same, albeit with some differences in phase (resulting in some time shift). In particular, only the right portion has a relative peak at the same time of the resistivity results (i.e. with a relative maximum at 3:25 am on 1st July), while on the left part it occurs at the time before. This, as well as the higher average temperature, may be related to a combination of local factors and, again, to the presence of the emissary of the small lakes upstream. This similarity between the DTS and the modelled ERT variations may indicate that the two processes can be described, in a first approximation, by the same equation but, at the same time, it also indicates that heat transport cannot be accurately described by the ADE equation, even though advection appears to be the controlling mechanism.

6. Conclusions

The characterization of the hyporheic and riparian zones of a river is a goal shared by several disciplines, given the pivotal role of these domains in the river ecosystem. The ERT and DTS implementation presented in this work, based on the innovative and (relatively) minimally invasive positioning of the instrumentation beneath the riverbed, demonstrates the high adaptability of these techniques and allow us not only to characterize the subsoil structure, but also to monitor the variations occurring on an hourly basis under the direct influence of the river stage changes. Moreover, the development of a hydrological model based on the ERT results helps understanding the hydrological properties and the processes taking place in the analyzed domain.

The most important scientific result in terms of process understanding is the demonstration that the water exchanges between the river and the hyporheic zone are in the present case extremely fast, and monitoring must be conducted on an hourly basis or less to capture the dynamics. Wider intervals in monitoring would cause time aliasing of the data and produce wrong images of the system dynamics: aliasing would convert the real high frequency response of the hyporheic zone in apparent lower frequency behaviors that might be mistaken for real to a naïve interpreter.

Another major advance of this work is the instrumentation set-up per se, which allows the acquisition of spatially distributed datasets, furthermore with a high spatial resolution. This instrumentation positioning should be carefully considered when dealing with domains that not only develop with depth (where the application of vertical boreholes is encouraged), but that also show features that vary laterally. In this case, in fact, the number of boreholes required could be substantially reduced (we drilled only one horizontal borehole instead of three/four vertical boreholes on the embankments and/or on the riverbed). Moreover, the geophysical datasets thus obtained give a new point of view on domains that otherwise would be impossible to describe spatially on a 2D section, since the presence of the creek represents an obstacle to the instrumentation placing (e.g. fixing the electrodes position on the riverbed during the time-lapse monitoring, digging vertical boreholes within the riverbed, etc.).

Finally, the combination of the geophysical results with hydrological data into a flow and transport model shows, once again, the potentiality of this approach in describing the processes occurring in the subsurface. Even if our analysis is not based on a coupled data assimilation approach, it provides very useful results, especially in relation to the subriverbed processes. This could lead to a deeper understanding of the structures and processes of the hyporheic and riparian zones, with important consequences on the river ecosystem management.

Supplementary data to this article can be found online at https://doi.org/10.1016/j.scitotenv.2018.08.179.

Acknowledgements

This work was supported by the EU 7th Framework Programme project GLOBAQUA ("Managing the effects of multiple stressors on aquatic ecosystems under water scarcity") [grant number 603629], the EU Framework Programme 7 Collaborative Project "CLIMB: Climate Induced Changes on the Hydrology of Mediterranean Basins: Reducing Uncertainty and Quantifying Risk through an Integrated Monitoring and Modeling System" for Theme 6.3 Environmental Technologies [Call ENV.2009.1.1.5.2, grant number 244151], the "Innovative methods for water resources management under hydro-climatic uncertainty scenarios, University of Trento, University of Padova, University of Naples, University of Modena-Reggio, Polytechnic of Milan, University of Roma "Roma Tre", CNR-ISAC Turin" project, funded by MIUR-PRIN [prot. 2010JHF437] and the "Hydro-geophysical monitoring and modelling for the Earth's Critical Zone" project, funded by the University of Padua [prot. CPDA147114].

References

Anderson, M.P., 2005. Heat as a ground water tracer. Groundwater 43 (6), 951–968. https://doi.org/10.1111/j.1745-6584.2005.00052.x.

Anderson, R.B., Naftz, D.L., Day-Lewis, F.D., Henderson, R.D., Stolp, D.O., Jewell, P., 2014. Quantity and quality of groundwater discharge in a hypersaline lake environment. J. Hydrol. 512, 177–194. https://doi.org/10.1016/j.jhydrol.2014.02.040.

Archie, G.E., 1942. The electrical resistivity log as an aid in determining some reservoir characteristics. Trans. AIME 146 (01), 54–62.

Bianchin, M., Smith, L., Beckie, R., 2010. Quantifying hyporheic exchange in a tidal river using temperature time series. Water Resour. Res. 46 (7). https://doi.org/10.1029/2009WR008365.

Binley, A., 2015. Tools and techniques: DC electrical methods. In: Schubert, G. (Ed.), Treatise on Geophysics, 2nd edition vol. 11. Elsevier, pp. 233–259. https://doi.org/10.1016/B978-0-444-53802-4.00192-5.

Binley, A., 2016. R2 code. http://www.es.lancs.ac.uk/people/amb/Freeware/R2/R2.htm, Accessed date: April 2016.

Binley, A.M., Kemna, A., 2005. DC resistivity and induced polarization methods. In: Rubin, Y., Hubbard, S.S. (Eds.), Hydrogeophysics, Water Sci. Technol. Library, Ser. 50. Springer, New York, pp. 129–156.

Binley, A., Ramirez, A., Daily, W., 1995. Regularised image reconstruction of noisy electrical resistance tomography data. In: Beck, M.S., Hoyle, B.S., Morris, M.A., Waterfall, R.C., Williams, R.A. (Eds.), Process Tomography, Proceedings of the 4th Workshop of the European Concerted Action on Process Tomography, Bergen, 6–8 April 1995, pp. 401–410.

Binley, A., Cassiani, G., Deiana, R., 2010. Hydrogeophysics: opportunities and challenges. Boll. Geofis. Teor. Appl. 51 (4).

Binley, A., Hubbard, S.S., Huisman, J.A., Revil, A., Robinson, D.A., Singha, K., Slater, L.D., 2015. The emergence of hydrogeophysics for improved understanding of subsurface processes over multiple scales. Water Resour. Res., 51 https://doi.org/10.1002/2015WR017016.

Blokhina, S., 2014. Risposta idrologica di recessione e morfologia della rete di drenaggio. University of Padua (PhD Thesis).

Boulton, A., Findlay, S., Marmonier, P., Stanley, E., Valett, H., 1998. The functional significance of the hyporheic zone in streams and rivers. Annu. Rev. Ecol. Syst. 29, 59–81. https://doi.org/10.1146/annurev.ecolsys.29.1.59.

Bridge, J.W., 2005. High Resolution In-situ Monitoring of Hyporheic Zone Biogeochemistry. Science Report SC030155/SR3. Environment Agency, Bristol, UK (51 pp.).

Briggs, M.A., Lautz, L.K., McKenzie, J.M., 2012a. A comparison of fibre-optic distributed temperature sensing to traditional methods of evaluating groundwater inflow to streams. Hydrol. Process. 26 (9), 1277–1290. https://doi.org/10.1002/hyp.8200.

Briggs, M.A., Lautz, L.K., McKenzie, J.M., Gordon, R.P., Hare, D.K., 2012b. Using high-resolution distributed temperature sensing to quantify spatial and temporal variability in vertical hyporheic flux. Water Resour. Res. 48 (2). https://doi.org/10.1029/2011WR011227.

Briggs, M.A., Voytek, E.B., Day-Lewis, F.D., Rosenberry, D.O., Lane, J.W., 2013. Understanding water column and streambed thermal refugia for endangered mussels in the Delaware River. Environ. Sci. Technol. 47 (20), 11423–11431. https://doi.org/10.1021/es4018893.

Busato, L., Boaga, J., Peruzzo, L., Himi, M., Cola, S., Bersan, S., Cassiani, G., 2016. Combined geophysical surveys for the characterization of a reconstructed river embankment. Eng. Geol. 211, 74–84. https://doi.org/10.1016/j.enggeo.2016.06.023.

Cardenas, M.B., Markowski, M.S., 2010. Geoelectrical imaging of hyporheic exchange and mixing of river water and groundwater in a large regulated river. Environ. Sci. Technol. 45 (4), 1407–1411. https://doi.org/10.1021/es103438a.

Cassiani, G., Bruno, V., Villa, A., Fusi, N., Binley, A.M., 2006. A saline trace test monitored via time-lapse surface electrical resistivity tomography. J. Appl. Geophys. 59, 244–259. https://doi.org/10.1016/j.jappgeo.2005.10.007.

Castellarin, A., Dal Piaz, G. V., Picotti, V., Selli, L., Cantelli, L., Martin, S., Montresor, L., Rigatti, G., Prosser, G., Bollettinari, G., Pellegrini, G. B., Carton, A., and Nardin, M., 2005. Note Illustrative della Carta Geologica d'Italia alla scala 1: 50.000, Foglio 059 Tione di Trento. Provincia Autonoma di Trento, Trento.

Constantz, J., 2008. Heat as a tracer to determine streambed water exchanges. Water Resour. Res. 44 (4). https://doi.org/10.1029/2008WR006996.

Coscia, I., Greenhalgh, S.A., Linde, N., Doetsch, J., Marescot, L., Günther, T., Vogt, T., Green, A.G., 2011. 3D crosshole ERT for aquifer characterization and monitoring of infiltrating river water. Geophysics 76 (2), G49–G59. https://doi.org/10.1190/1.3553003.

Coscia, I., Linde, N., Greenhalgh, S., Vogt, T., Green, A., 2012. Estimating traveltimes and groundwater flow patterns using 3D time-lapse crosshole ERT imaging of electrical resistivity fluctuations induced by infiltrating river water. Geophysics 77 (4), E239–E250. https://doi.org/10.1190/geo2011-0328.1.

Crook, N., Zarnetske, J., Haggerty, R., Robinson, D.A., Binley, A., Knight, R., 2010. Electrical resistivity imaging of the architecture of substream sediments. Water Resour. Res. 46. https://doi.org/10.1029/2008WR006968 (11 pp.).

Daily, W., Ramirez, A., LaBrecque, D., Nitao, J., 1992. Electrical resistivity tomography of vadose water movement. Water Resour. Res. 28, 1429–1442. https://doi.org/10.1029/91WR03087.

Daily, W., Ramirez, A., Binley, A., LeBrecque, D., 2004. Electrical resistance tomography. Lead. Edge 23, 438–442. https://doi.org/10.1190/1.1729225.

Dal Piaz, G.V., Castellarin, A., Martin, S., Selli, L., Carton, A., Pellegrini, G.B., Casolari, E., Daminato, F., Montresor, L., Picotti, V., Prosser, G., Santuliana, E., and Cantelli, L., 2007. Note Illustrative della Carta Geologica d'Italia alla scala 1: 50.000, Foglio 042 Malé. Provincia Autonoma di Trento, Servizio Geologico. APAT, Servizio Geologico d'Italia, Roma, 143.

Doetsch, J., Linde, N., Vogt, T., Binley, A., Green, A.G., 2012. Imaging and quantifying salt-tracer transport in a riparian groundwater system by means of 3D ERT monitoring. Geophysics 77 (5), B207–B218. https://doi.org/10.1190/geo2012-0046.1.

Doro, K.O., Leven, C., Cirpka, O.A., 2013. Delineating subsurface heterogeneity at a loop of river Steinlach using geophysical and hydrogeological methods. Environ. Earth Sci. 69 (2), 335–348. https://doi.org/10.1007/s12665-013-2316-0.

Dugdale, S.J., Hannah, D.M., Malcolm, I.A., 2017. River temperature modelling: a review of process-based approaches and future directions. Earth Sci. Rev. 175, 97–113. https://doi.org/10.1016/j.earscirev.2017.10.009.

Fleckenstein, J.H., Krause, S., Hannah, D.M., Boano, F., 2010. Groundwater-surface water interactions: new methods and models to improve understanding of processes and dynamics. Adv. Water Resour. 33 (11), 1291–1295. https://doi.org/10.1016/j.advwatres.2010.09.011.

Gooseff, M.N., Anderson, J.K., Wondzell, S.M., LaNier, J., Haggerty, R., 2006. A modelling study of hyporheic exchange pattern and the sequence, size, and spacing of stream bedforms in mountain stream networks, Oregon, USA. Hydrol. Process. 20 (11), 2443–2457. https://doi.org/10.1002/hyp.6349.

Graves, P.R., Gardiner, D.J., 1989. Practical Raman Spectroscopy. Springer-Verlag.

Greswell, R.B., 2005. High-resolution In Situ Monitoring of Flow Between Aquifers and Surface Water, Science Report SC030155/SR4. Environment Agency, Bristol, UK (38 pp.).

Hem, J.D., 1985. Study and Interpretation of the Chemical Characteristics of Natural Water. vol. 2254. Department of the Interior, US Geological Survey.

Holz, M., Heil, S.R., Sacco, A., 2000. Temperature-dependent self-diffusion coefficients of water and six selected molecular liquids for calibration in accurate ^{1}H NMR PFG measurements. Phys. Chem. Chem. Phys. 2 (20), 4740–4742. https://doi.org/10.1039/B005319H.

Hurtig, E., Großwig, S., Kühn, K., 1996. Fibre optic temperature sensing: application for subsurface and ground temperature measurements. Tectonophysics 257 (1), 101–109. https://doi.org/10.1016/0040-1951(95)00124-7.

Johnson, T.C., Slater, L.D., Ntarlagiannis, D., Day-Lewis, F.D., Elwaseif, M., 2012. Monitoring groundwater-surface water interaction using time-series and time-frequency analysis of transient three-dimensional electrical resistivity changes. Water Resour. Res. 48 (7). https://doi.org/10.1029/2012WR011893.

LaBrecque, D.J., Miletto, M., Daily, W., Ramirez, A., Owen, E., 1996. The effects of noise on Occam's inversion of resistivity tomography data. Geophysics 61 (2), 538–548. https://doi.org/10.1190/1.1443980.

Lautz, L.K., Siegel, D.I., 2006. Modeling surface and ground water mixing in the hyporheic zone using MODFLOW and MT3D. Adv. Water Resour. 29 (11), 1618–1633. https://doi.org/10.1016/j.advwatres.2005.12.003.

Lesmes, D.P., Friedman, S.P., 2005. Relationships between the electrical and hydrogeological properties of rocks and soils. Hydrogeophysics. Springer, Dordrecht, pp. 87–128.

Lin, H.C., Richards, D.R., Yeh, G.T., Cheng, J.R., Chang, H.P., Jones, N.L., 1996. FEMWATER: A Three-dimensional Finite Element Computer Model for Simulating Density Dependent Flow and Transport. Technical Report. U.S. Army Eng. Waterways Exp. Station, Vicksburg, Miss (129 pp.).

Ludwig, R., Soddu, A., Duttmann, R., Baghdadi, N., Benabdallah, S., Deidda, R., Marrocu, M., Strunz, G., Wendland, F., Engin, G., Paniconi, C., Prettenthaler, F., Lajeunesse, I., Afifi, S., Cassiani, G., Bellin, A., Mabrouk, B., Bach, H., Ammerl, T., 2010. Climate-induced changes on the hydrology of mediterranean basins - a research concept to reduce uncertainty and quantify risk. Fresenius Environ. Bull. 19 (10A), 2379–2384.

Monego, M., Cassiani, G., Deiana, R., Putti, M., Passadore, G., Altissimo, L., 2010. Tracer test in a shallow heterogeneous aquifer monitored via time-lapse surface ERT. Geophysics 75, WA61–WA73. https://doi.org/10.1190/1.3474601.

Mwakanyamale, K., Slater, L., Day-Lewis, F., Elwaseif, M., Johnson, C., 2012. Spatially variable stage-driven groundwater-surface water interaction inferred from time-frequency analysis of distributed temperature sensing data. Geophys. Res. Lett. 39 (6). https://doi.org/10.1029/2011GL050824.

Nash, J.E., Sutcliffe, J.V., 1970. River flow forecasting through conceptual models part I—a discussion of principles. J. Hydrol. 10 (3), 282–290. https://doi.org/10.1016/0022-1694(70)90255-6.

Navarro-Ortega, A., Acuña, V., Bellin, A., Burek, P., Cassiani, G., Choukr-Allah, R., Dolédec, S., Elosegi, A., Ferrari, F., Ginebreda, A., Grathwohl, P., Jones, C., Ker Rault, P., Kok, K., Koundouri, P., Ludwig, R.P., Merz, R., Milacic, R., Muñoz, I., Nikulin, G., Paniconi, C., Paunović, M., Petrovic, M., Sabater, L., Sabater, S., Skoulikidis, N.Th., Slob, A., Teutsch, G., Voulvoulis, N., Barceló, Damià, 2015. Managing the effects of multiple stressors on aquatic ecosystems under water scarcity. The GLOBAQUA project. Sci. Total Environ. 504, 3–9. https://doi.org/10.1016/j.scitotenv.2014.06.081.

Nyquist, J.E., Freyer, P.A., Toran, L., 2008. Stream bottom resistivity tomography to map ground water discharge. Ground Water 46, 561–569. https://doi.org/10.1111/j.1745-6584.2008.00432.x.

Nyquist, J.E., Heaney, M.J., Toran, L., 2009. Characterizing lakebed seepage and geologic heterogeneity using resistivity imaging and temperature measurements. Near Surf. Geophys. 7 (5–6), 487–498. https://doi.org/10.3997/1873-0604.2009022.

Orghidan, T., 2010. A new habitat of subsurface waters: the hyporheic biotope. Fundam. Appl. Limnol. 176, 291–302. https://doi.org/10.1127/1863-9135/2010/0176-0291.

Perri, M.T., De Vita, P., Masciale, R., Portoghese, I., Chirico, G.B., Cassiani, G., 2018. Time-lapse Mise-á-la-Masse measurements and modelling for tracer test monitoring in a shallow aquifer. J. Hydrol. 561, 461–477. https://doi.org/10.1016/j.jhydrol.2017.11.013.

Raman, C.V., Krishnan, K.S., 1928. A new type of secondary radiation. Nature 121 (3048). https://doi.org/10.1038/121501c0.

Reidy, C., Clinton, S., 2004. Down Under: Hyporheic Zones and Their Function. Center for Water and Watershed Studies, University of Washington, Seattle.

Rubin, Y., Hubbard, S.S., 2005. Hydrogeophysics. Water Science and Technology Library. vol. 50. Springer, Netherlands, p. 523.

Selker, J.S., Thevenaz, L., Huwald, H., Mallet, A., Luxemburg, W., Van De Giesen, N., Stejskal, M., Zeman, J., Westhoff, M., Parlange, M.B., 2006. Distributed fiber-optic temperature sensing for hydrologic systems. Water Resour. Res. 42 (12). https://doi.org/10.1029/2006WR005326.

Sen, P.N., Goode, P.A., Sibbit, A., 1988. Electrical conduction in clay bearing sandstones at low and high salinities. J. Appl. Phys. 63 (10), 4832–4840. https://doi.org/10.1063/1.340476.

Servizio Geologico – Provincia autonoma di Trento, 2017. Carta Tecnica 2017 (Servizio di download). http://www.territorio.provincia.tn.it/portal/server.pt/community/carta_tecnica_provinciale/920/carta_tecnica_provinciale/40052, Accessed date: 11 May 2017.

Siergieiev, D., Ehlert, L., Reimann, T., Lundberg, A., Liedl, R., 2015. Modelling hyporheic processes for regulated rivers under transient hydrological and hydrogeological conditions. Hydrol. Earth Syst. Sci. 19 (1), 329. https://doi.org/10.5194/hess-19-329-2015.

Slater, L.D., Ntarlagiannis, D., Day-Lewis, F.D., Mwakanyamale, K., Versteeg, R.J., Ward, A., Strickland, C., Johnson, C.D., Lane, J.W., 2010. Use of electrical imaging and distributed temperature sensing methods to characterize surface water–groundwater exchange regulating uranium transport at the Hanford 300 Area, Washington. Water Resour. Res. 46 (10). https://doi.org/10.1029/2010WR009110.

Terzaghi, K., Peck, R.B., Mesri, G., 1996. Soil Mechanics in Engineering Practice. John Wiley & Sons.

Tonina, D., Buffington, J.M., 2007. Hyporheic exchange in gravel bed rivers with pool-riffle morphology: laboratory experiments and three-dimensional modeling. Water Resour. Res. 43 (1). https://doi.org/10.1029/2005WR004328.

Tyler, S.W., Selker, J.S., Hausner, M.B., Hatch, C.E., Torgersen, T., Thodal, C.E., Schladow, S.G., 2009. Environmental temperature sensing using Raman spectra DTS fiber-optic methods. Water Resour. Res. 45 (4). https://doi.org/10.1029/2008WR007052.

Vignoli, G., Gervasio, I., Brancatelli, G., Boaga, J., Della Vedova, B., Cassiani, G., 2016. Frequency-dependent multi-offset phase analysis of surface waves: an example of high resolution characterization of a riparian aquifer. Geophys. Prospect. 64 (1), 102–111. https://doi.org/10.1111/1365-2478.12256.

Vogt, T., Schneider, P., Hahn-Woernle, L., Cirpka, O.A., 2010. Estimation of seepage rates in a losing stream by means of fiber-optic high-resolution vertical temperature profiling. J. Hydrol. 380 (1–2), 154–164. https://doi.org/10.1016/j.jhydrol.2009.10.033.

Voytek, E.N., Drenkelfuss, A., Day-Lewis, F.D., Healy, R., Lane, J.W., Werkema, D., 2014. 1DTempPro: analyzing temperature profiles for groundwater/surface-water exchange. Ground Water 52 (2), 298–302. https://doi.org/10.1111/gwat.12051.

Ward, A.S., Gooseff, M.N., Singha, K., 2010. Characterizing hyporheic transport processes—interpretation of electrical geophysical data in coupled stream–hyporheic zone systems during solute tracer studies. Adv. Water Resour. 33 (11), 1320–1330. https://doi.org/10.1016/j.advwatres.2010.05.008.

Ward, A.S., Gooseff, M.N., Singha, K., 2013. How does subsurface characterization affect simulations of hyporheic exchange? Groundwater 51 (1), 14–28. https://doi.org/10.1111/j.1745-6584.2012.00911.x.

Waxman, M.H., Smits, L.J.M., 1968. Electrical conductivities in oil-bearing shaly sands. Soc. Pet. Eng. J. 8 (02), 107–122. https://doi.org/10.2118/1863-A.

Westhoff, M.C., Savenije, H.H.G., Luxemburg, W.M.J., Stelling, G.S., van de Giesen, N.C., Selker, J.S., Pfister, L., Uhlenbrook, S., 2007. A distributed stream temperature model using high resolution temperature observations. Hydrol. Earth Syst. Sci. 11, 1469–1480. https://doi.org/10.5194/hess-11-1469-2007.

Westhoff, M.C., Gooseff, M.N., Bogaard, T.A., Savenije, H.H.G., 2011. Quantifying hyporheic exchange at high spatial resolution using natural temperature variations along a first-order stream. Water Resour. Res. 47. https://doi.org/10.1029/2010WR009767 (n/a-n/a).